SENCKENBERG

ORIGINAL PAPER

Late Devonian (Famennian) to Carboniferous (Mississippian-Pennsylvanian) conodonts from the Anarak section, Central Iran

Elahe Sattari[1] · Ali Bahrami[1] · Peter Königshof[2] · Hossein Vaziri-Moghaddam[1]

Abstract

A relatively complete conodont record from Famennian to the Mississippian/Pennsylvanian boundary was investigated in the Anarak section, Central Iran. The studied interval belongs to the Bahram, Shishtu, Ghaleh and Absheni formations. The Famennian part of the section (Bahram Formation) ranges from the *Palmatolepis triangularis* Zone into the *Bispathodus ultimus* Zone. Not all conodont zones could be defined due to the lack of indicative species. Furthermore, it seems likely that a hiatus occurs around the Devonian/Carboniferous (D/C) boundary (most probably from the *Siphonodella praesulcata* to the ?*Siphonodella sulcata*–early *Siphonodella crenulata* conodont zones) based on the lack of stratigraphically important conodonts as well as on sedimentological criteria. The lack of representative siphonodellids and protognathodids at the base of the Mississippian prevents detailed stratigraphic position of the D/C boundary. Lower Carboniferous (Mississippian) rocks are characterized by red nodular limestone which is unique in comparison with other studied sections of the same age in Central Iran. Within the studied section, we could define the Mississippian/Pennsylvanian boundary. The mid-Carboniferous boundary was defined by the occurrence of *Declinognathus noduliferus* s.l. Conodont biofacies changes (Mississippian genera *Gnathodus* and *Lochriea* have been replaced by Pennsylvanian genera *Declinognathus* and *Idiognathodus*) are recognized in this section as well.

Keywords Biostratigraphy · Devonian · Carboniferous · Anarak · Central Iran

Introduction

The mid-Palaeozoic, particularly the Devonian/Carboniferous (D/C), transition was a critical interval in Earth's history which was characterized by dramatic climate and faunal

✉ Ali Bahrami
a.bahrami@sci.ui.ac.ir; Bahrami_geo@yahoo.com

✉ Peter Königshof
peter.koenigshof@senckenberg.de

Elahe Sattari
elahehsatari1987@gmail.com

Hossein Vaziri-Moghaddam
avaziri7304@gmail.com

[1] Department of Geology, Faculty of Sciences, University of Isfahan, Isfahan, Iran

[2] Senckenberg Research Institute and Natural History Museum, Senckenberganlage 25, 60325 Frankfurt am Main, Germany

changes, severe anoxic intervals, frequent sea level changes and intensified volcanism which finally led from global greenhouse conditions to icehouse conditions (Caplan et al. 1996; Caplan and Bustin 1999; Streel et al. 2000; Joachimski and Buggisch 2002; Joachimski et al. 2004, 2006; Kaiser et al. 2006, 2011; Buggisch et al. 2008; Caputo et al. 2008; Isaacson et al. 2008; Marynowski et al. 2012; Kumpan et al. 2014a, b; Paschall et al. 2019). The first-order mass extinction at the end of the Devonian (Hangenberg Crisis) caused not only a loss of major fossil groups such as conodonts (the main extinction among conodonts occurred during the global deposition of the Hangenberg Black Shale, see review by Kaiser et al. 2016) but also entire ecosystems such as metazoan reefs. In the aftermath of the Kellwasser Crisis around the Frasnian/Famennian boundary, the reefs were significantly reduced but no reef complex survived the Hangenberg Crisis (e.g. Webb 2002). The D/C transition is characterized by several transgressive/regressive cycles, and widespread ocean anoxia have been recognized along continental margins or epicontinental basins known as the Hangenberg Black Shale

(HBS) Event. Close to the D/C boundary, a major sea level fall (Hangenberg Sandstone Event, HSS) can be recognized in many sections around the world. This eustatic sea level fall is most probably associated with a glaciation on Gondwana (e.g. Caputo 1985; Isaacson et al. 1999, 2008; Streel et al. 2000, 2001; Caputo et al. 2008; Brezinski et al. 2008, 2010; Lakin et al. 2016). The Mississippian shows a transition between early Palaeozoic stable warm and greenhouse conditions to more late Palaeozoic oscillating climates, including several major glacial episodes (e.g. Powell 2005, 2007; Kammer and Ausich 2006; Montanez et al. 2007; Mullins and Servais 2008; Heim 2009; Lowry et al. 2014; Sardar Abadi et al. 2017).

Glacial deposits have been reported from the Viséan and Serpukhovian with a maximum extent during the Bashkirian and the Moskovian (Garzanti and Sciunnach 1997; López-Gamundi 1997; López-Gamundi and Martínez 2000). It is believed that the Late Palaeozoic Ice Age (LPIA) is one of the most important ice ages that cover much of the Late Devonian to Permian when the ice waxed and waned across southern Gondwana (Veevers and Powell 1987). The LPIA consisted of several discrete glacial climates with warmer periods of glacial minima. Ice minimum and maximum intervals were reported from low latitudes (e.g. Soreghan and Giles 1999; Bischoff et al. 2009, 2010) as well as from high latitudes (e.g. Caputo et al. 2008; Isbell et al. 2008a, b).

During the Palaeozoic, Iran was part of the northern margin of Gondwana. Marine conditions occurred in Northern and Central Iran from the Middle Devonian to Early Frasnian and persisted into the Early Pennsylvanian (Berberian and King 1981; Husseini 1991; Sharland et al. 2001). A widespread uplift during the latest Carboniferous led to continental environments before the onset of a new marine cycle during the Early Permian. The entire sequence from the Late Devonian, Carboniferous into the Permian deposits of Central Iran is divided into five lithostratigraphic units: the Bahram Formation (Givetian–Famennian), the Shishtu Formation (Tournaisian–Serpukhovian), the Sardar Group (Bashkirian–Moscovian), the Zaladu Formation (Gzhelian–Asselian) and the Jamal Formation (Permian).

The first detailed data on the Upper Devonian to Lower Permian successions in Central and Eastern Iran were obtained during the geological mapping of the Tabas and Kerman areas (Huckriede et al. 1962; Stöcklin et al. 1965; Ruttner and Stöcklin 1966; Ruttner et al. 1968; Stöcklin 1968, 1971; Stepanov 1971; Walliser 1984; Weddige 1984). More recently, numerous publications provided comprehensive stratigraphic and palaeontologic data about this region (Korn et al. 1999; Yazdi 1999; Wendt et al. 2002, 2005; Leven and Gorgij 2009; Leven et al. 2006; Hairapetian et al. 2006; Hashemie et al. 2015). Bahrami et al. (2014) described the first conodont data from the Mississippian/Pennsylvanian boundary interval in Central Iran. The aim of this study is to describe new conodont assemblages from the Late Devonian (Famennian) to the Mississippian/Pennsylvanian boundary of the Anarak section.

Geological setting

The Anarak area belongs to the NW part of the Central-East Iranian Microcontinent, which is juxtaposed with the Great
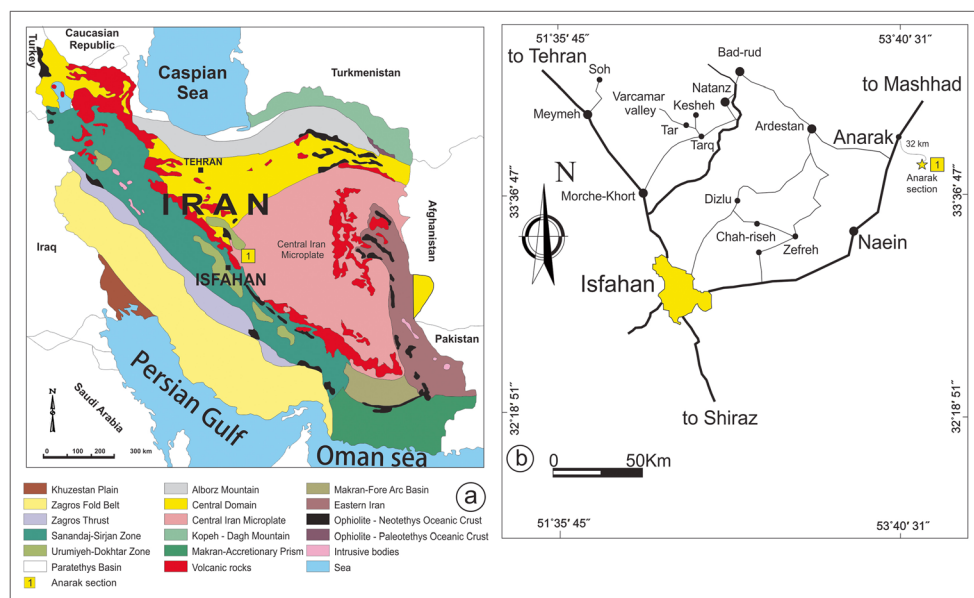
Fig. 1 a Structural units of Iran and location (1) of the Anarak section. **b** Road map showing the position of the Anarak section northeast of Isfahan (modified after Bakhtiari 2005)
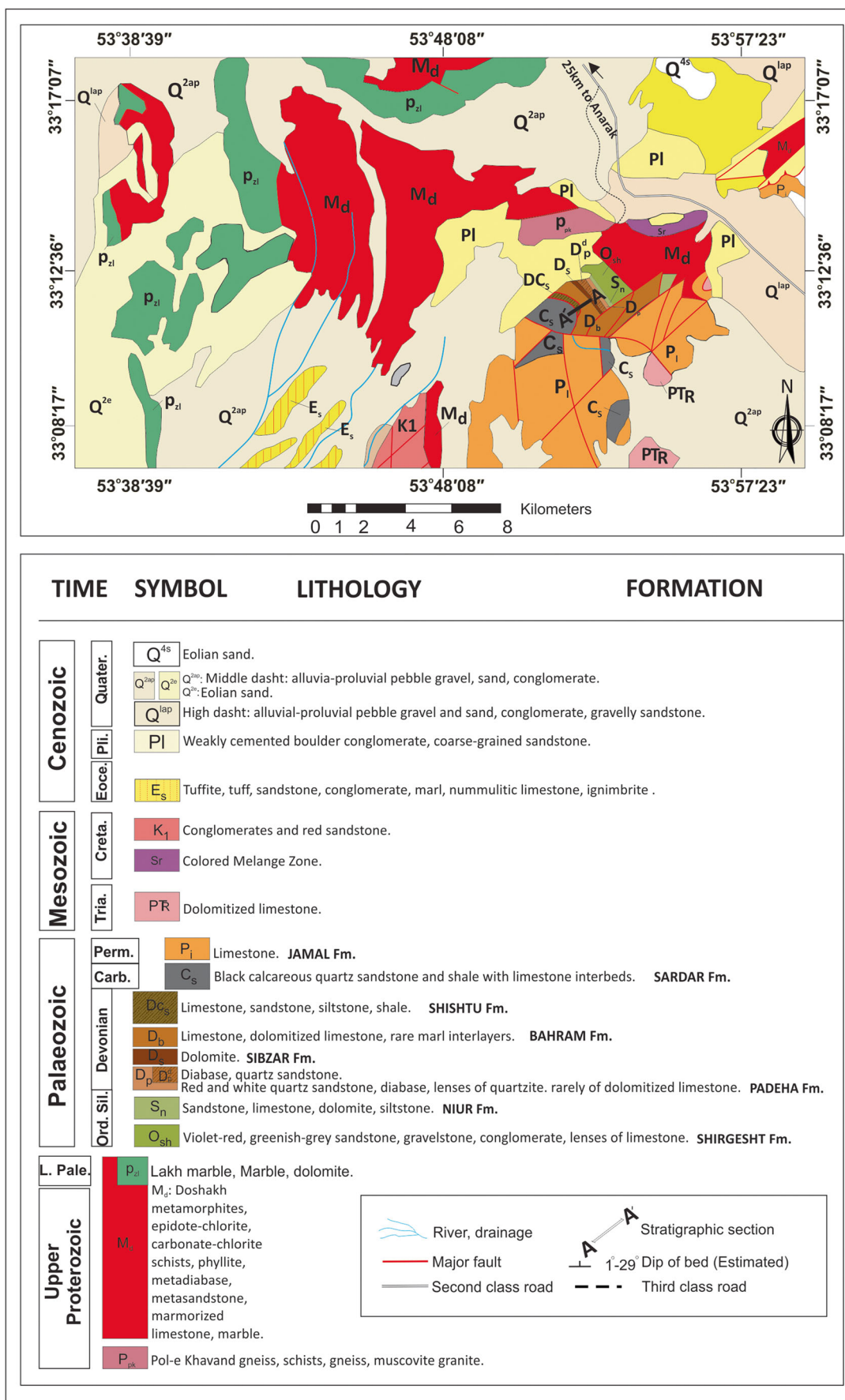
Fig. 2 Geological map and location of the investigated section A`—A (modified after Sharkovski et al. 1984)

Kavir Block and the Sanandaj–Sirjan Zone, is characterized by a complex tectonic history (Davoudzadeh et al. 1981; Soffel et al. 1996; Korn et al. 1999; Bagheri and Stampfli 2008). The section is composed of a 5000–8000-m-thick series of sedimentary, volcanoclastic and metamorphic rocks (Soffel et al. 1996; Almasian 1997; Korn et al. 1999; Leven et al. 2006; Aghanabati 2010).

The latter ones contain marbles, schists, gneisses and meta-diabases which are unconformably overlain by a series of approximately 1200-m-thick Palaeozoic sediments, ranging stratigraphically from the Ordovician Shirgesht Formation to the Permian Jamal Formation (Lensch and Davoudzadeh 1982; Leven et al. 2006; Hairapetian et al. 2015). Major crustal movements associated with basaltic and ultrabasic volcanism and deposition of preferably shallow-marine deposits led to a complex geology exposed in this area. Several thrust, horst and graben structures and lateral facies changes occur. The entire succession contains some hiatuses due to erosion and/or tectonic uplift.

The section described here (Figs. 1 and 2) is located close to the northern end of the N–S striking mountain range Kuh-e-Bande-Abdol-Hossein which is located southwest of the Kuh-e-Lakh metamorphosed complex, about 34 km southwest of Anarak (sheet 6756 Anarak, 1:100,000; WGS coordinates: base

of the section 33° 10′ 44.79″ N, 53° 52′ 23.83″ E; top of the section 33° 10′ 33.78″ N, 53° 52′ 22.90″ E; see Figs. 1 and 2).

The base of the section is composed of 700 m of volcanic and sedimentary deposits of ?Late Cambrian–Late Ordovician age (Hairapetian et al. 2015). These series rests upon the Doshakh metamorphic complex (Sharkovski et al. 1984; Schallreuter et al. 2006; Muttoni et al. 2009). The overlaying sedimentary sequence belongs to the carbonate–siliciclastic deposits of the Silurian Niur Formation. Intercalated in this succession are volcanic rocks, such as basalts. Reddish sediments of the Lower to Middle Devonian Padeha Formation with intercalated volcanic rocks at the base cover this succession. The Padeha Formation is commonly overlain by dolostones of the Sibzar Formation which gradually passes into limestones of the Bahram Formation (Bahrami et al. 2014). The Late Devonian (Famennian) Bahram Formation is conformably overlain by the Early Mississippian Shishtu Formation which is composed of red, marly limestones.

Some limestones are rich in fossils and provided an age range from Viséan to late Namurian (Korn et al. 1999). The red nodular limestones are conformably overlain by a cliff-forming, coarse and poorly sorted limestone breccia. The topmost part is composed of Upper Mississippian (Viséan–

Table 1 Stratigraphy and formations applied to the Upper Devonian–Permian strata of Central-Eastern Iran, modified after Leven et al. (2006)

		Central and East Iran			Alburz	
		Anarak-Yazd-Tabas		Kerman-Kalmard	central	eastern
Permian	Asselian	Zaladu Formation		Khan	Dorud	
Carboniferous / Pennsylvanian	Gzhelian	Zaladu Formation		Khan	Dorud	
Carboniferous / Pennsylvanian	Kasimovian	/////		/////	/////	/////
Carboniferous / Pennsylvanian	Moscovian	Sardar Group "Sardar1" "Sardar2"	Absheni Formation	Hutk/Gachal	Bagher-Abad	Ghesel - Ghaleh
Carboniferous / Pennsylvanian	Bashkirian	Sardar Group "Sardar1" "Sardar2"	Ghaleh Formation	Hutk/Gachal	Bagher-Abad	Ghesel - Ghaleh
Carboniferous / Mississippian	Serpukhovian	Shishtu		Hutk/Gachal	Mobarak	Ghesel - Ghaleh
Carboniferous / Mississippian	Visean	Shishtu		Hutk/Gachal	Mobarak	Ghesel - Ghaleh
Carboniferous / Mississippian	Tournasian	Shishtu		Hutk/Gachal	Mobarak	Ghesel - Ghaleh
Devonian / Late	Famennian	Bahram		Zarand / Rahdar	Jeirud	Khoshyeilagh
Devonian / Late	Frasnian	Bahram		Zarand / Rahdar	Jeirud	Khoshyeilagh
Devonian / Middle	Givetian	Sibzar		Zarand / Rahdar	Jeirud	Khoshyeilagh

Table 2 Conodont element distribution and number of elements of the Anarak section (Devonian part, samples A2–A29)

Anarak section	A2	A3	A4	A5	A6	A7	A8	A9	A10	A11	A12	A13	A14	A15	A16	A17	A18	A19	A20	A21	A22	A23	A24	A25	A26	A27	A28	A29	Total
Alternognathus regularis regularis																				2									2
Ancyrognathus sinelaminus									1	1	1																		3
Bispathodus aculeatus aculeatus																								1	4		1	7	13
Bispathodus bispathodus																							5		1			12	18
Bispathodus cf. costatus																									1			1	2
Bispathodus cf. ultimus																										1			1
Bispathodus costatus																								1	1			6	8
Bispathodus jugosus																							2		1				3
Bispathodus spinulicostatus																									1	1	3		5
Bispathodus stabilis stabilis																						2	1	11					14
Bispathodus stabilis vulgaris																				1	1	3							5
Bispathodus ultimus																										1			1
Branmehla bohlenana																				1			1						2
Clydagnathus ormistoni																							1		1				2
Icriodus alternatus alternatus										1	1	1	1	1	5	8													18
Icriodus alternatus helmsi											1	1	2	1															5
Icriodus cf. cornutus																	1	2											3
Icriodus cornutus																	1	1			1								3
Icriodus costatus darbyensis																											1	1	2
Mehlina strigosa																	1		2		1								4
Palmatolepis glabra pectinata																1	1	1											3
Palmatolepis gracilis expansa																							1		1	1			3
Palmatolepis gracilis gracilis														1	1														2
Palmatolepis gracilis sigmoidalis																				1		3							4
Palmatolepis minuta loba													3	4	1														8
Palmatolepis minuta minuta															1		1	3		5									10
Palmatolepis perlobata maxima																	1	1	1										3
Palmatolepis perlobata perlobata												1	1																2
Palmatolepis quadrantinodosalobata																	2	1											3
Palmatolepis triangularis																													4
Pelekysgnathus inclinatus										3		1																	4
Polygnathus aequalis	3	1	1																										5

Table 2 (continued)

Anarak section	A2	A3	A4	A5	A6	A7	A8	A9	A10	A11	A12	A13	A14	A15	A16	A17	A18	A19	A20	A21	A22	A23	A24	A25	A26	A27	A28	A29	Total
Polygnathus aff. *subnormalis*																1	1												2
Polygnathus aspelundi aspelundi						1		5																					6
Polygnathus brevilaminus							1	1		1	2	5																	10
Polygnathus cf. *alatus*	2	1	1	1	3																								8
Polygnathus cf. *politus*	4	3	1	3	1																								12
Polygnathus cf. *xylus*	5	11	2																										18
Polygnathus communis collinsoni																											1	7	8
Polygnathus delicatulus																									1				1
Polygnathus granulosus																				3									3
Polygnathus inconcinnus																		1	1										2
Polygnathus nodocostatus																			1	1									2
Polygnathus padovanii																	3												3
Polygnathus perplexus																				1					1				2
Polygnathus semicostatus															1	3	5		1	2									12
Polygnathus tichonovitchi												1																	1
Polygnathus triphylatus																		2	1										3
Polygnathus webbi	1	1	3	6	1																								12
Pseudopolygnathus primus																									1	1	1		3
Scaphignathus velifer leptus																					1	1							2
Scaphignathus velifer velifer																				1	5								6
Total	15	17	8	10	5	1	4	7	4	4	6	9	6	7	8	15	11	10	14	14	18	6	20	2	14	5	7	34	292

Namurian) grey fossiliferous thick-bedded calcareous mudstone (Sharkovski et al. 1984). Leven et al. (2006) studied the Pennsylvanian succession (Sardar Group) of the Anarak section. The Sardar Group (previously Sardar Formation) is divided into two formations: the Ghaleh Formation (formerly "Sardar 1", early Bashkirian age), which is mainly composed of carbonate, and the siliciclastic or mixed carbonate–siliciclastic Absheni Formation (formerly "Sardar 2", early Moscovian; see Table 1).

Material and methods

In order to improve and update the biostratigraphy of the Anarak section, fifty-six conodont samples of approximately 4 to 5 kg each were taken from carbonate rock and processed by standard methods (see Jeppsson and Anehus 1995). The process was repeated until samples were dissolved. The washed residues were dried in an oven (~ 40 °C) and later sieved and separated into three different fractions. Conodonts were handpicked utilizing a binocular microscope. Depending on the depositional facies setting, the number of conodonts per sample was highly variable; e.g. in dolostones, no conodonts were found whereas in shallow-water limestones, a good number of species occurred in distinct horizons. Herein, the conodont zonation scheme follows Ziegler

and Sandberg (1990), Lane et al. (1999), Kaiser et al. (2009), Hartenfels (2011) and Spalletta et al. (2017). A total number of 373 conodonts were obtained from the residues which led to the identification of 71 species and subspecies within eighteen genera: *Alternognathus*, *Ancyrognathus*, *Bispathodus*, *Branmehla*, *Clydagnathus*, *Declinognathus*, *Idiognathus*, *Gnathodus*, *Locheria*, *Icriodus*, *Mehlina*, *Palmatolepis*, *Pelekysgnathus*, *Polygnathus*, *Protognathodus*, *Pseudopolygnathus*, *Rhachistognathus* and *Scaphignathus* (Tables 2 and 3). Overall, the preservation of the conodont elements was good, and several specimens are broken or incomplete as a result of sediment transport. The conodont collection is stored at the Department of Geology (sample numbers: EUIC), University of Isfahan, Islamic Republic of Iran. Repository numbers of the figured specimens are given in the explanations of plates. The colour alteration of conodonts (CAI, Epstein et al. 1977) in the Givetian and Frasnian limestones is CAI 4–4.5 (Shakeri 2017), whereas in the Famennian and Mississippian, the colour gradually changes to lower CAI of 2–2.5.

Lithology

Based on field observations and sedimentological characteristics, the Anarak section was subdivided in five units, which are

Table 3 Conodont element distribution and number of elements of the Anarak section (Carboniferous part, samples A30–A53)

Anarak section	A30	A31	A32	A33	A34	A35	A36	A37	A38	A39	A46	A47	A48	A49	A50	A51	A25	A53	Total
Declinognathodus noduliferus														3	3	1			7
Declinognathodus praenoduliferus														1	1	1			3
Gnathodus bilineatus									1										1
Gnathodus cuneiformis			1	1	2														4
Gnathodus delicatus			1	1	1														3
Gnathodus girtyi girtyi											1	2	2						5
Gnathodus girtyi simplex							1				1	1	1						3
Gnathodus pseudosemiglaber							5	7											12
Gnathodus semiglaber			1	1	1	3	2												8
Gnathodus typicus			1	1	1	2													5
Idiognathodus sinuosus																1	1		2
Locheria commutata									1	1									2
Polygnathus inornatus	2	1																	3
Polygnathus inornatus inornatus	1	1	1																3
Polygnathus longiposticus	1	1	1																4
Polygnathus parapetus		1																	3
Protognathodus collinsoni																			1
Rachistognathus minutus minutus																1	1	3	5
Rachistognathus muricatus											3	1	3						7
Total	5	6	3	4	4	5	11	9	2	1	5	4	6	4	4	3	2	4	81
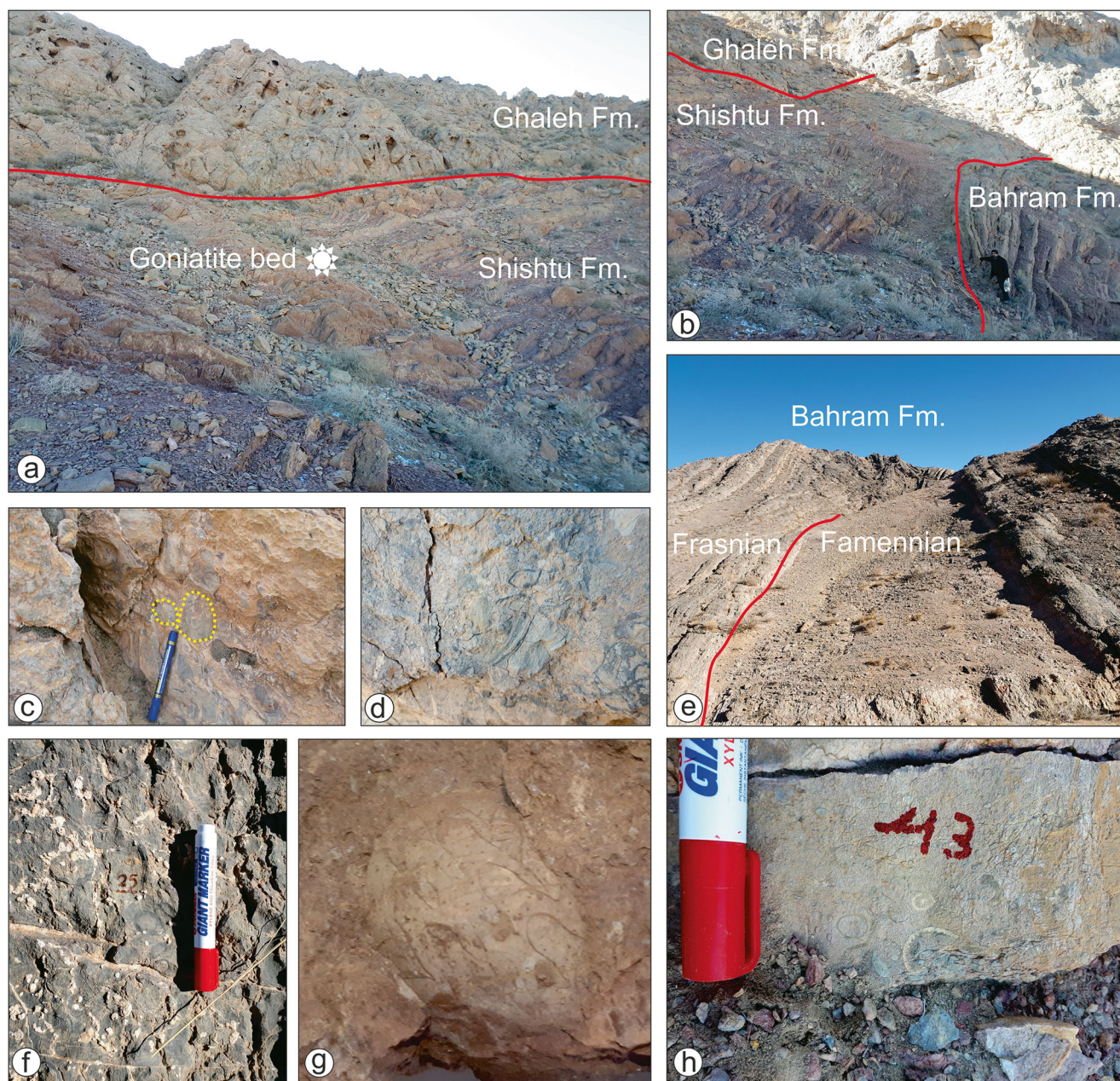
Fig. 3 **a**, **b**, **e** Panoramic views of the studied interval (Bahram, Shishtu and Ghaleh formations). **c** Cliff-forming brecciated grey to whitish limestone (package 4). **d** Grey, fossiliferous thick-bedded limestone (package 5). **f** Grey skeletal limestone (package 3). **g** Goniatite bearing red marly nodular limestone at the top of package 3. **h** Thin-bedded grey fossiliferous limestone including, corals and brachiopod shells in package 3

summarized from base to top (Figs. 3 and 4). It is not the aim of this paper to provide a detailed sedimentological analysis which will be published elsewhere. The base of the section (package 1, samples A1–A6, thickness 15 m) starts with grey, medium to thick-bedded fossiliferous limestone. This succession is conformably overlain mainly by greyish to white, thin-bedded nodular limestone (package 2, samples A7–A29, thickness 30 m). The portion contains some reddish shale horizons with grade upwards into skeletal limestone. These sediments are overlain by red, nodular limestone which yielded a number of macrofossils, such

as gastropods, brachiopods and solitary corals (package 3, samples A30–A48, thickness 68 m). Three meters below the top, a 20-cm-thick marker horizon with goniatites occurs. The next succession (package 4, samples A49–A50, thickness 27 m) is mainly composed of whitish, cliff-forming brecciated limestone and dolostone with rare macro fossils which is overlain by grey, fossiliferous thick-bedded mudstone and limestone (package 5, samples A51–A56, thickness 38 m). Some sedimentological characteristics are shown in Fig. 3.
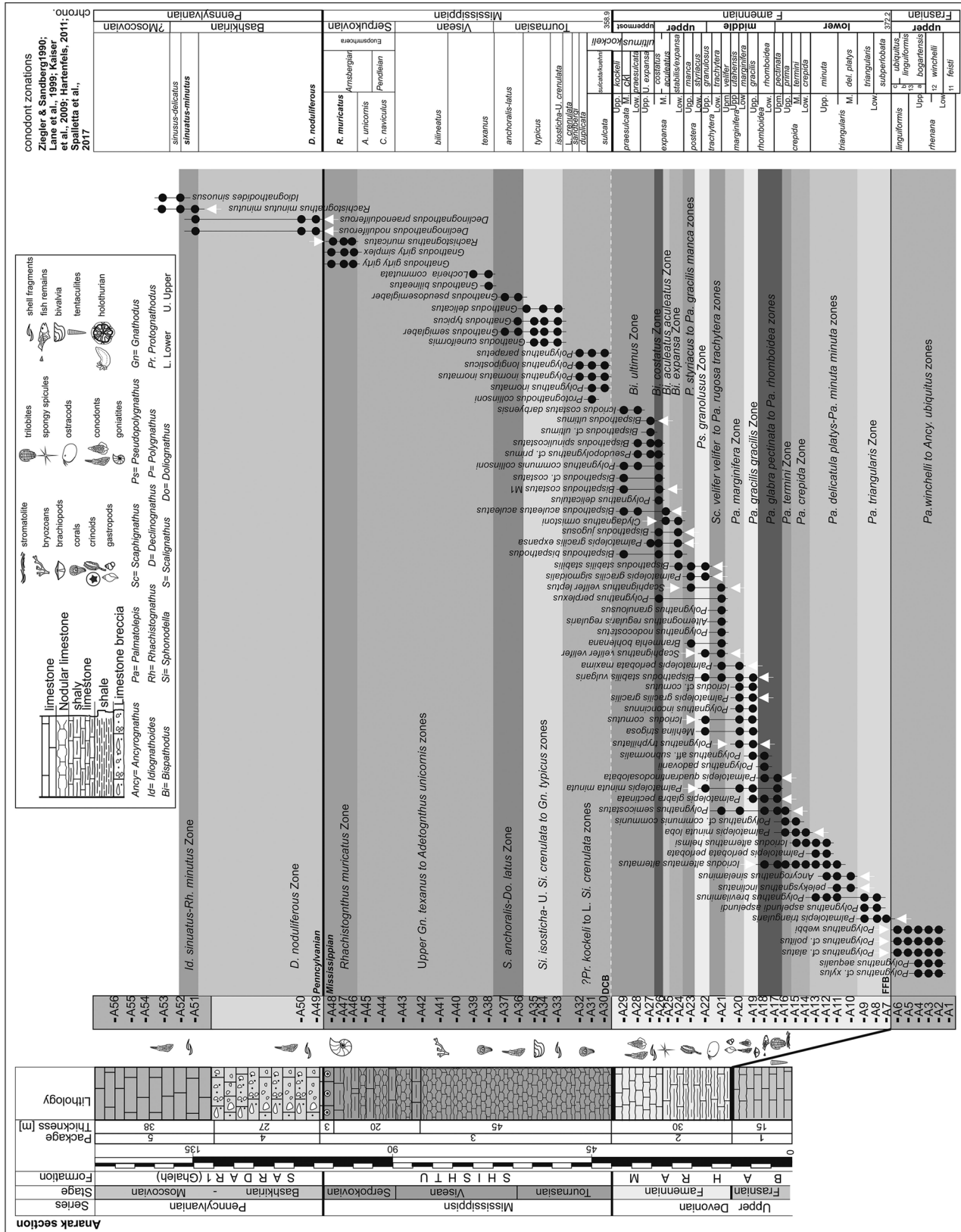
Fig. 4 Stratigraphic log, samples position, conodont occurrences and biozonation of Anarak section
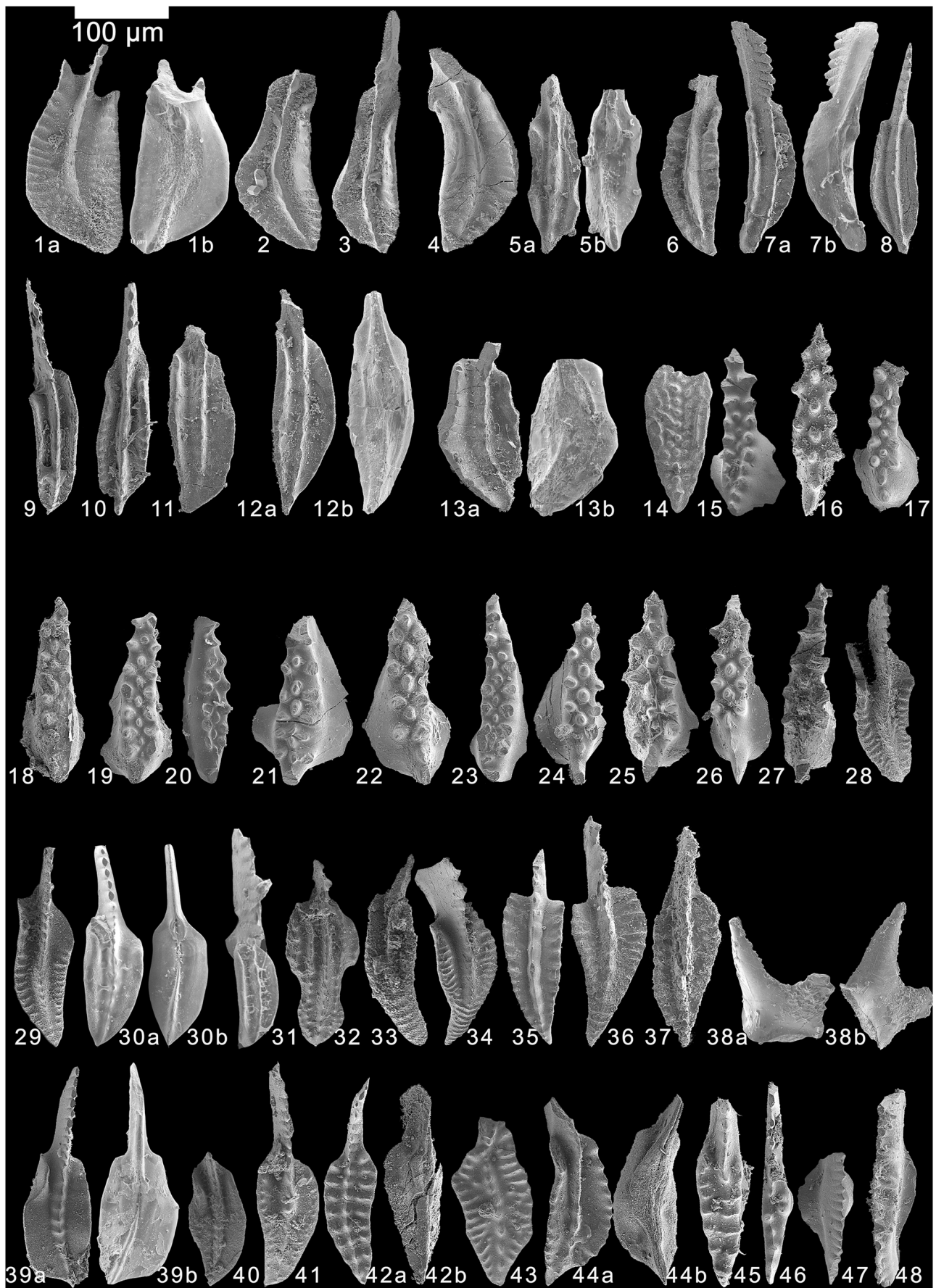
◀ **Fig. 5** Conodonts from the Anarak section, with a given scale bar of 100 μm. *1 Polygnathus webbi* Stauffer, 1938; upper (a) and lower (b) views of IUMC 200, sample A4. *2, 3 Polygnathus aequalis* Klapper & Lane, 1985; *2* upper view of IUMC 201, sample A4; *3* upper view of IUMC 202, sample A4. *4 Polygnathus alatus* Huddle, 1934; upper view of IUMC 203, sample A4. *5 Polygnathus* cf. *xylus* Stauffer, 1938; upper (a) and lower (b) views of IUMC 204, sample A4. *6, 7 Polygnathus aequalis* Klapper & Lane, 1985; *6* upper-oblique view of IUMC 205, sample A2; *7* upper (a) and lower (b) views of IUMC 206, sample A3. *8 Polygnathus brevilaminus* Branson & Mehl, 1934a; upper view of IUMC 207, sample A13. *9, 10 Polygnathus aspelundi aspelundi* Savage & Funai, 1980; *9* upper view of IUMC 208, sample A9; *10* upper view of IUMC 209, sample A8. *11–12 Polygnathus* cf. *politus* Ovnatanova, 1969; *11* upper view of IUMC 210, sample A2. *12* Upper (a) and lower (b) views of IUMC 211, sample A6. *13 Polygnathus* cf. *alatus* Huddle 1934; upper (a) and lower (b) views of IUMC 212, sample A4. *14 Ancyrognathus sinelaminus* (Branson and Mehl, 1934); upper view of IUMC 213, sample A10. *15 Icriodus alternatus helmsi*, Sandberg et Dreesen, 1984; upper view of IUMC 214, sample A15. *16–21 Icriodus alternatus alternatus* Branson & Mehl, 1934; *16* upper view of IUMC 215, sample A11; *17* upper view of IUMC 216, sample A12; *18* upper view of IUMC 217, sample A13; *19* upper view of IUMC 218, sample A14; *20* upper-oblique view of IUMC 219, sample A15; *21* upper view of IUMC 220, sample A16. *22, 23 Icriodus alternatus helmsi*, Sandberg and Dreesen 1984; *22* upper view of IUMC 221, sample A12; *23* upper view of IUMC 222, sample A13. *24, 25 Icriodus costatus darbyensis* Klapper 1958; *24* upper view of IUMC 223, sample A28; *25* upper view of IUMC 224, sample A29. *26 Icriodus* cf. *cornutus* Sannemann, 1955; upper lateral view of IUMC 225, sample A19. *27 Icriodus cornutus* Sannemann, 1955; upper view of IUMC 226, sample A22. *28, 29 Polygnathus padovanii*, Perri and Spalletta 1990; *28* upper view of IUMC 227, sample A18; *29* upper view of IUMC 228, sample A18. *30, 31 Polygnathus communis communis* Branson & Mehl, 1934; *30* upper (a) and lower (b) views of IUMC 229, sample A15; *31* upper-oblique view of IUMC 230, sample A15. *32 Polygnathus triphylatus* Helms, 1961; upper view of IUMC 231, sample A19. *33–36 Polygnathus semicostatus* Branson and Mehl, 1934; *33* upper view of IUMC 232, sample A21; *34* upper lateral view of IUMC 233, sample A21; *35* upper view of IUMC 234, sample A16; *36* upper view of IUMC 235, sample A17. *37 Polygnathus delicatulus* Ulrich and Bassler 1926; upper view of IUMC 236, sample A26. *38 Pelekysgnathus inclinatus* Thomas 1949; upper-oblique (a) and lateral (b) views of IUMC 237, sample A10. *39, 40 Polygnathus communis collinsoni* Druce 1969; *39* upper (a) and lower (b) views of IUMC 238, sample A26; *40* upper view of IUMC 239, sample A29. *41 Polygnathus* sp. Upper view of IUMC 236, sample A22. *42 Alternognathus regularis regularis* Ziegler and Sandberg 1984; upper (a) and lower (b) views of IUMC 237, sample A21. *43 Polygnathus tichonovitchi* Kuzmin & Melinkova, 1991; upper view of IUMC 238, sample A13. *44 Polygnathus* aff. *subnormalis* Vorontsova and Kuzmin 1984; upper (a) and lower (b) views of IUMC 239, sample A18. *45 Scaphignathus velifer velifer* Helms 1959; upper view of IUMC 240, sample A21. *46* Gen. et sp. indet. Upper view of IUMC 241, sample A25. *47, 48 Bispathodus stabilis vulgaris* (Dzik 2006) Branson & Mehl, 1934; *47* upper view of IUMC 242, sample A21; *48* upper lateral view of IUMC 243, sample A22

Conodont succession

Although carbonate samples of 4 to 5 kg per sample were dissolved for biostratigraphic analysis, the overall number of conodont elements is relatively low as it was shown in other shallow-water sections, for instance, by Bahrami et al. (2018, 2019) and Ariuntogos et al. (in press). As a result, we are not able to recognize all of the conodont zones used in the revised Conodont Standard Zonation (see Hartenfels 2011; Spalletta et al. 2017). As it is common practice in high-resolution stratigraphic conodont studies, only Pa elements were identified, as many multielement reconstructions are still doubtful and incomplete. However, studied conodont elements lead to the discrimination of 22 biostratigraphic intervals (Fig. 4).

Palmatolepis winchelli to *Ancyrognathus ubiquitus* zones (samples A2–A6)

Although the indicative species *Palmatolepis winchelli*, *Palmatolepis bogartensis* and *Ancyrognathus ubiquitus* (Girard et al. 2005) are absent, the upper boundary of this biozone corresponds to the last occurrence of *Polygnathus* cf. *politus* Ovanatanova 1969; *Polygnathus webbi* Stauffer 1938; and *Polygnathus* cf. *alatus* Huddle 1934 in level A6 in our section. All mentioned species become extinct in the *linguiformis* Zone (Ziegler and Sandberg 1996, 2000; Ovnatanova and Kononova 2001, 2008; Bultynck 2003). Therefore, this assemblage belongs to an Upper Frasnian, Upper *rhenana-linguiformis* interval or more updated global biozones *Palmatolepis winchelli* to *Ancyrognathus ubiquitus*. *Polygnathus aequalis* and *Polygnathus* cf. *xylus* are the other important associated species. The Frasnian–Famennian boundary of the Anarak section seems to be continues with no interruptions, no evidence of any disconformity observed in the field which means lithologically the F/F boundary does not show characteristic sediments, such as black limestones or black shales as it is known from many places around the world (see Carmichael et al. 2019), which is a result of overall shallow-water palaeoenvironment. For more detailed conodont biostratigraphic framework and biofacies analysis of the Givetian and Frasnian part of the Anarak section (Kuh-e-Bande-Abdol-Hossein), see Bahrami et al. (2019).

Palmatolepis triangularis Zone (samples A7–A9)

Spalletta et al. (2017) proposed the *Palmatolepis subperlobata* Zone which correlates with the lowest part of the former Lower *triangularis* Zone. The new base is defined by the first appearance datum (FAD) of *Palmatolepis subperlobata*. Within the studied section (samples A7–A9), the index conodont *Palmatolepis subperlobata* was not observed. Thus, the lowermost part of the Famennian according to the new standard zonation (Spalletta et al. 2017) was not proven by conodonts. The base of this following interval was recognized by the entry of *Palmatolepis triangularis* Sannemann 1955a in level A7. This zone corresponds to the upper part of the former Lower *triangularis* Zone. The top is defined by the entry of *Pelekysgnathus inclinatus* Thomas 1949 and *Ancyrognathus sinelaminus* (Branson and Mehl 1934a)
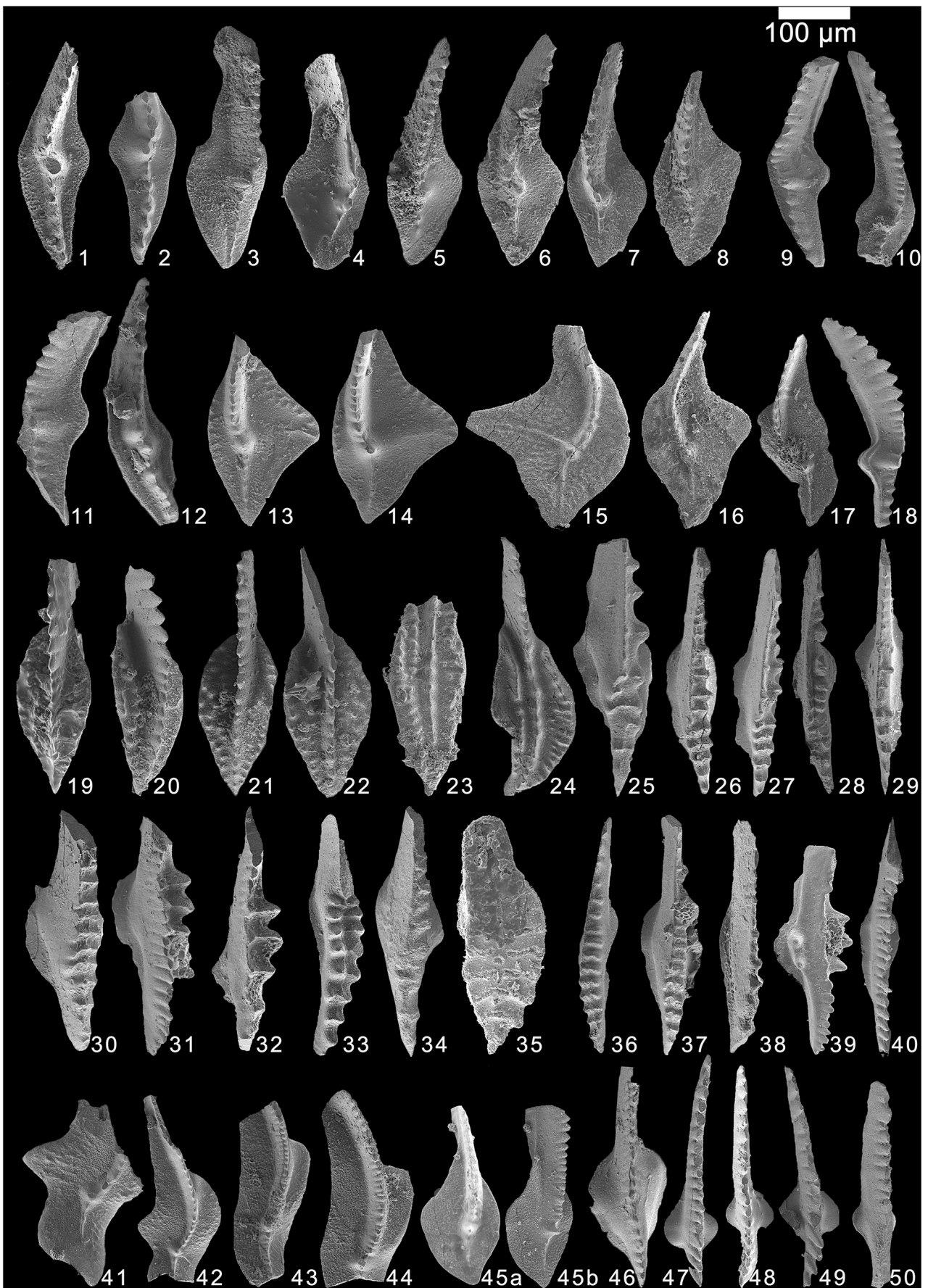
◀ **Fig. 6** Conodonts from the Anarak section, with a given scale bar of 100 μm. *1, 2 Palmatolepis gracilis expansa* Sandberg and Ziegler, 1979 M1; *1* upper view of IUMC 244, sample A24; *2* upper view of IUMC 245, sample A26. *3–8 Palmatolepis minuta minuta* Branson & Mehl, 1934a; *3* upper view of IUMC 246, sample A17; *4* upper view of IUMC 247, sample A17; *5* upper view of IUMC 248, sample A22; *6* upper view of IUMC 249, sample A22; *7* upper view of IUMC 250, sample A22; *8* upper lateral view of IUMC 251, sample A22. *9–11 Palmatolepis gracilis sigmoidalis* Ziegler, 1962a; *9* upper lateral view of IUMC 252, sample A22; *10* upper view of IUMC 253, sample A22; *11* upper view of IUMC 254, sample A23. *12 Palmatolepis gracilis gracilis* Branson & Mehl, 1934a; upper view of IUMC 255, sample A19. *13, 14 Palmatolepis minuta loba* Helms, 1963; *13* upper view of IUMC 256, sample A14; *14* upper view of IUMC 257, sample A15. *15 Palmatolepis quadrantinodosalobata* Sannemann, 1955a; upper view of IUMC 258, sample A17. *16 Palmatolepis triangularis* Sannemann, 1955; upper view of IUMC 259, sample A7. *17 Palmatolepis perlobata perlobata* Ulrich and Basller, 1926; upper view of IUMC 260, sample A12. *18 Palmatolepis gracilis sigmoidalis* Ziegler, 1962a; upper lateral view of IUMC 261, sample A22. *19, 20 Polygnathus perplexus*, Thomas, 1949; *19* upper lateral view of IUMC 262, sample A21; *20* upper lateral view of IUMC 263, sample A26. *21, 22 Polygnathus granulosus*, Branson & Mehl, 1934a; *21* upper view of IUMC 264, sample A21; *22* upper view of IUMC 265, sample A21. *23 Polygnathus nodocostatus* Branson & Mehl, 1934; upper view of IUMC 266, sample A21. *24 Polygnathus inconcinnus* Kuzmin & Melnikova, 1991; upper view of IUMC 267, sample A19. *25 Bispathodus ultimus* Bischoff, 1957; upper view of IUMC 268, sample A27. *26, 27 Bispathodus bispathodus* Ziegler, Sandberg and Austin, 1974; *26* upper lateral view of IUMC 269, sample A26; *27* upper lateral view of IUMC 270, sample A29. *28 Bispathodus costatus* (Branson, 1934) morphotype 1; upper lateral view of IUMC 271, sample A25. *29 Bispathodus bispathodus* Ziegler, Sandberg and Austin, 1974; upper view of IUMC 272, sample A26. *30 Bispathodus* cf. *ultimus* Bischoff, 1957; upper view of IUMC 273, sample A27. *31 Bispathodus aculeatus aculeatus* Branson & Mehl, 1934a; upper lateral view of IUMC 274, sample A25. *32 Bispathodus spinulicostatus* (Branson, 1934) morphotype 1; upper lateral view of IUMC 275, sample A26. *33 Scaphignathus velifer velifer* Helms, 1959; upper view of IUMC 276, sample A22. *34 Bispathodus* cf. *costatus* Branson, 1934; upper lateral view of IUMC 277, sample A26. *35 Bispathodus* cf. *ultimus* Bischoff, 1957; upper view of IUMC 278, sample A27. *36 Scaphignathus velifer leptus* Ziegler & Sandberg, 1984. Upper view of IUMC 279, sample A23. *37 Bispathodus jugosus* (Branson & Mehl, 1934a); upper view of IUMC 280, sample A24. *38 Bispathodus bispathodus* Ziegler, Sandberg and Austin, 1974; *20* upper lateral view of IUMC 281, sample A26. *39 Pseudopolygnathus primus* Branson & Mehl, 1934b; upper view of IUMC 282, sample A27. *40 Bispathodus stabilis vulgaris* Dzik, 2006; upper view of IUMC 283, sample A21. *41, 42 Palmatolepis perlobata maxima* Müller, 1956; *41* upper view of IUMC 284, sample A19; *42* upper view of IUMC 285, sample A19. *43, 44 Palmatolepis glabra pectinata* Ziegler, 1962; *43* upper view of IUMC 286, sample A17, X 127; *44* upper view of IUMC 287, sample A17, X 138. *45 Palmatolepis minuta minuta* Branson & Mehl, 1934a; upper (a) and upper lateral (b) views of IUMC 288, sample A22. *46 Bispathodus stabilis stabilis* (Branson & Mehl, 1934a); upper lateral view of IUMC 289, sample A22. *47–50 Branmehla bohlenana* (Helms, 1959); *47* upper view of IUMC 290, sample A21; *48* upper view of IUMC 291, sample A21; *49* upper view of IUMC 292, sample A21; *50* upper view of IUMC 293, sample A21

at the base of the next zone. *Polygnathus brevilaminus* and *Polygnathus asplundi asplundi* were also recovered in this zone (Fig. 5).

Palmatolepis delicatula platys to *Palmatolepis minuta minuta* zones (samples A10–A13)

The *Palmatolepis delicatula platys* Zone corresponds exactly to the former Middle *triangularis* Zone of Ziegler and Sandberg 1990. We did not find the zonal name-given conodont species, but the base of this interval (sample A10) was discriminated by the first occurrence of *Pelekysgnathus inclinatus* Thomas 1949 which ranges from Middle *triangularis* Zone to Upper *praesulcata* Zone (Sandberg and Dreesen 1984; Huang and Gong 2016) and *Ancyrognathus sinelaminus* Branson and Mehl 1934a which ranges from the Middle *triangularis* Zone into the Uppermost *crepida* Zone (Ziegler and Sandberg 1990). *Palmatolepis perlobata perlobata* Ulrich and Bassler 1926 enters in level A12 which is the other important indicator to define the lower limit of this interval. *Icriodus alternatus alternatus* and *Icriodus alternatus helmsi* were the other species recovered in this interval.

## *Palmatolepis crepida* Zone (samples A14–A15)

The *Palmatolepis crepida* Zone corresponds to the former Lower *crepida* Zone (Ziegler and Sandberg 1990), and the base can be discriminated by the first appearance of *Palmatolepis minuta loba* Helms 1963 which ranges from the base of the *P. crepida* Zone to *P. rhomboidea* Zone (Spalletta et al. 2017). *Icriodus alternatus helmsi* Sandberg and Dreesen 1984 become extinct at the end of this zone. Other associated species in level A14 are *Icriodus alternatus alternatus* and *Polygnathus* cf. *communis communis*.

Palmatolepis termini Zone (sample A16)

This interval is equivalent to the former Middle *crepida* Zone (Ziegler and Sandberg 1990). The base is characterized by the entry of *Polygnathus semicostatus* Branson and Mehl 1934a in level A16, which has its first occurrence within the *Palmatolepis termini* Zone of Spalletta et al. (2017) and extends into the *Bispathodus ultimus* Zone. *Palmatolepis minuta loba*, *Icriodus alternatus alternatus* and *Polygnathus* cf. *communis communis* are associated as well.

Palmatolepis glabra pectinata to *Palmatolepis rhomboidea* zones (samples A17–A18)

The base is well marked by the first occurrence of *Palmatolepis glabra pectinata* Ziegler, 1962b M1 Sandberg and Ziegler 1973 in level A17 and *Palmatolepis quadrantinodosalobata* Sannemann, 1955a M1 Sandberg
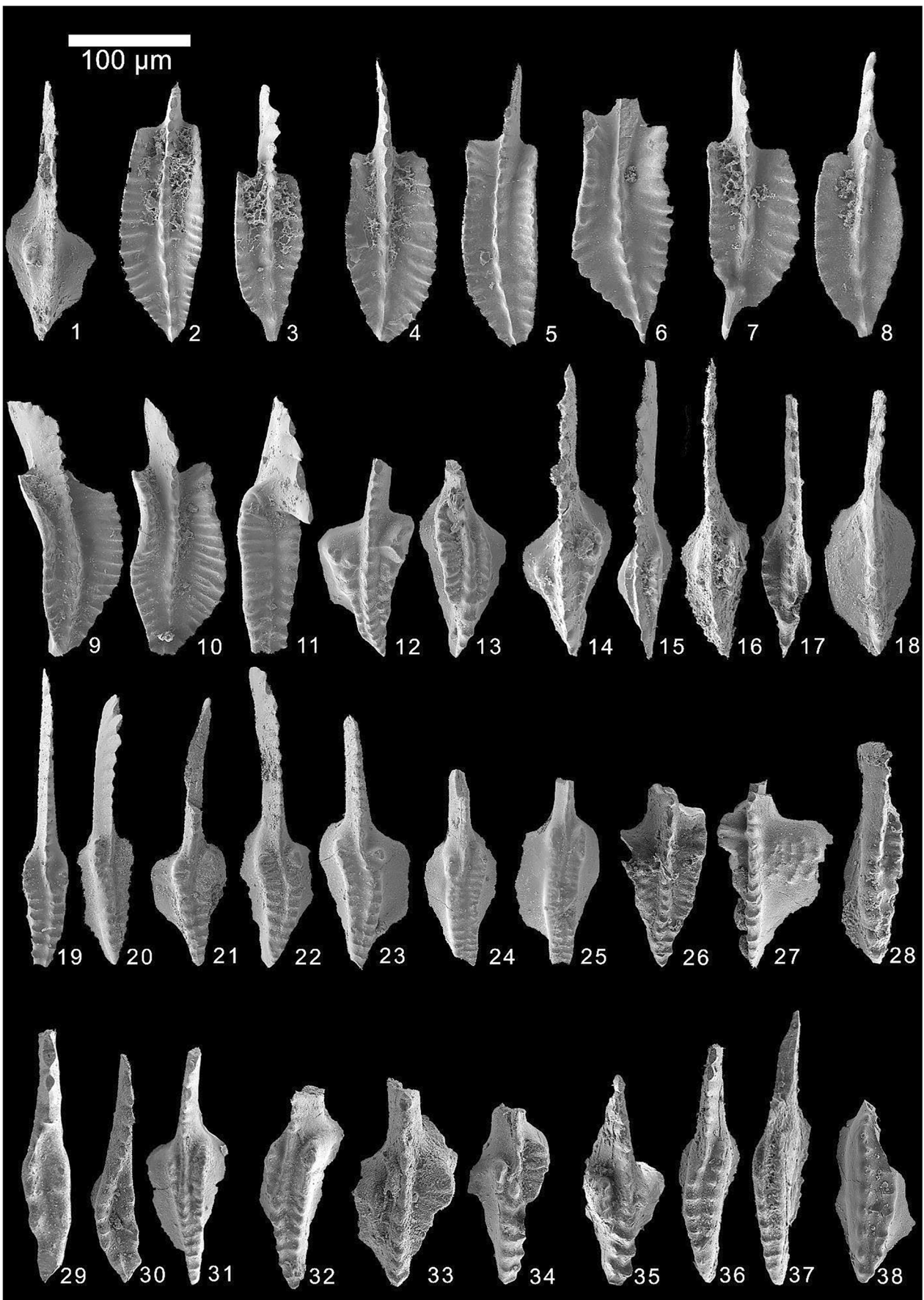
◄ Fig. 7 Conodonts from the Anarak section, with a scale bar given for each sample. *1 Protognathodus collinsoni* Ziegler, 1969; upper view of IUMC 294, sample A31. *2–5, 7, 8 Polygnathus inornatus inornatus* Branson, 1934; *2* upper view of IUMC 295, sample A30; *3* upper view of IUMC 296, sample A30; *4* upper view of IUMC 297, sample A31; *5* upper view of IUMC 298, sample A31; *7* upper view of IUMC 299, sample A30; *8* upper view of IUMC 300, sample A31. *6 Polygnathus longiposticus* Branson & Mehl, 1934; upper view of IUMC 301, sample A30. *9, 10 Polygnathus parapetus* Druce, 1969; *9* upper view of IUMC 302, sample A32; *10* upper view of IUMC 303, sample A31. *11 Clydagnathus ormistoni* Beinert, Klapper, Sandberg & Ziegler, 1971; upper view of IUMC 304, sample A24. *12 Gnathodus delicatus* Branson & Mehl, 1938; upper view of IUMC 305, sample A38. *13 Gnathodus girtyi simplex* Dunn, 1966; upper view of IUMC 306, sample A38. *14 Gnathodus typicus* Cooper, 1939; upper view of IUMC 307, sample A36. *15, 16 Gnathorius girtyi girtyi* Hass, 1953; *15* upper view of IUMC 308, sample A38; *16* upper view of IUMC 309, sample A38. *17 Gnathodus girtyi simplex* Dunn, 1966; upper view of IUMC 310, sample A38. *18 Lochriea commutata* (Branson & Mehl, 1941); upper view of IUMC 311, sample A39. *19–21 Declinognathodus praenoduliferus* Nigmadganov and Nemirovskaya, 1992; *19* upper view of IUMC 312, sample A49; *20* upper view of IUMC 313, sample A50; *21* upper view of IUMC 314, sample A50. *22–25 Declinognathodus noduliferus* s.l. (Ellison and Graves, 1941); *22* upper view of IUMC 315, sample A50; *23* upper view of IUMC 316, sample A51; *24* upper view of IUMC 317, sample A51; *25* upper view of IUMC 318, sample A49. *26 Gnathodus cuneiformis* Mehl & Thomas, 1947; upper view of IUMC 319, sample A35. *27 Gnathodus bilineatus bilineatus* Roundy, 1926; upper view of IUMC 320, sample A38. *28 Rachistognathodus minutus minutus* (Higgins & Bouckaert, 1968); upper lateral view of IUMC 321, sample A51. *29 Rachistognathodus minutas minutas* (Higgins & Bouckaert, 1968); upper lateral view of IUMC 322, sample A46. *30 Rachistognathodus muricatus* Dunn, 1966; upper view of IUMC 323, sample A48. *31, 32 Gnathodus girtyi girtyi* Hass, 1953; *31* upper view of IUMC 324, sample A38; *32* upper lateral view of IUMC 325, sample A38. *33 Gnathodus semiglaber* Bischoff, 1957; upper view of IUMC 326, sample A35. *34 Gnathodus pseudosemiglaber* Thomson and Fellow, 1970; upper lateral view of IUMC 327, sample A37. *35 Gnathodus pseudosemiglaber* Thomson and Fellow, 1970; upper view of IUMC 328, sample A37. *36 Gnathodus girtyi simplex* Dunn, 1966; upper view of IUMC 220, sample A39. *37, 38 Idiognathodus sinuosus* Ellison & Graves, 1941; *37* upper view of IUMC 329, sample A52; *38* upper view of IUMC 330, sample A52

and Ziegler 1973, and both species have their first occurrence in the *Palmatolepis glabra pectinata* Zone (Spalletta et al. 2017). *Icriodus alternatus alternatus* Branson & Mehl, 1934a, which become extinct at the top of this interval in level A18 (Bultynck 2003; Spalletta et al. 2017), is the other indicator for discriminating the upper boundary of this interval. *Polygnathus* cf. *communis communis*, *Polygnathus padovanii*, *Polygnathus* cf. *subnormalis* and *Palmatolepis minuta minuta* are also present.

Palmatolepis gracilis gracilis Zone (sample A19)

This interval corresponds to the former Upper *rhomboidea* Zone (Ziegler and Sandberg 1990). The lower limit can be identified by the first entry of *Palmatolepis gracilis gracilis* Branson & Mehl, 1934a and *Polygnathus triphylatus* Helms, 1961, and *Bispathodus stabilis vulgaris* in level A19, the first occurrence of all mentioned species, corresponds to the *Palmatolepis gracilis gracilis* Zone (see Metzger 1994; Klapper and Ziegler 1979; Spalletta et al. 2017). *Polygnathus semicostatus*, *Palmatolepis glabra pectinata*, *Palmatolepis minuta minuta*, *P. subnormalis*, *Mehlina strigosa*, *Icriodus cornutus* and *Polygnathus inconcinnus* are the other associated conodonts.

Palmatolepis marginifera marginifera Zone (sample A20)

This conodont zone in level A20 is confirmed by the first occurrence of *Palmatolepis perlobata maxima* Müller, 1956, which has its FAD within the lower part of this conodont zone (Spalletta et al. 2017). *Bispathodus stabilis vulgaris*, *Palmatolepis gracilis gracilis*, *Palmatolepis minuta minuta*, *Polygnathus semicostatus* and *Icriodus cornutus* are also present, and *Polygnathus triphylatus* Helms 1961 becomes extinct within the lower part of this conodont zone (Spalletta et al. 2017).

Scaphignathus velifer velifer to *Palmatolepis rugosa trachytera* zones (sample A21)

The base of this interval is well defined by the first entry of index species *Scaphignathus velifer velifer* Helms 1959 and *Scaphignathus velifer leptus* Ziegler & Sandberg, 1984, and both have their first occurrences in the *Scaphignathus velifer velifer* Zone (= former Uppermost *marginifera* Zone). The other associated species are *Polygnathus perplexus*, *Polygnathus granulosus*, *Alternognathus regularis regularis*, *Polygnathus nodocostatus*, *Branmehla bohlenana*, *Bispathodus stabilis vulgaris*, *Palmatolepis perlobata maxima*, *Mehlina strigosa* and *Polygnathus semicostatus*.

Pseudopolygnathus granulosus Zone (sample A22)

The base of this interval is coincident with the first entry of *Palmatolepis gracilis sigmoidalis* Ziegler, 1962a and *Bispathodus stabilis stabilis* (Branson & Mehl, 1934a) [M2], and the top limit can be fully identified by the last occurrence of *Icriodus cornutus* Sannemann, 1955b, *Palmatolepis minuta minuta* Branson & Mehl, 1934a and *Scaphignathus velifer velifer* Helms, 1959 in level A22 which all become extinct in the *granulosus* Zone (former Upper *trachytera* Zone) (see Bultynck 2003; Ji and Ziegler 1993; Ziegler and Sandberg 1984; Spalletta et al. 2017). *Bispathodus stabilis vulgaris* and *Mehlina strigosa* are also presented.

Polygnathus styriacus to *Palmatolepis gracilis manca* zones (sample A23)

Sample A23 yielded very few conodonts, and this interval is tentatively assigned between the lower and upper discriminated zones. *Scaphignathus velifer leptus* Ziegler & Sandberg, 1984 become extinct at the end of this interval in level A23. In fact, *Scaphignathus velifer leptus* ranges from the lower part of the *Scaphignathus velifer velifer* Zone to the top of the *Palmatolepis gracilis manca* Zone (Spalletta et al. 2017). *Bispathodus stabilis stabilis*, *Branmehla bohlenana* and *Palmatolepis gracilis sigmoidalis* are associated species.

Palmatolepis gracilis expansa Zone (sample A24)

The zone is equivalent to the former Lower *expansa* Zone. The entry of *Bispathodus jugosus* (Branson and Mehl 1934a) and *Palmatolepis gracilis expansa* (Sandberg and Ziegler 1979) in level A24, both range from the *P. gracilis expansa* into the *Bispathodus ultimus* of Spalletta et al. (2017), defines the base of this interval; associated species are *Clydagnathus ormistoni*, *Bispathodus bispathodus* and *Bispathodus stabilis stabilis* (Fig. 6).

Bispathodus aculeatus aculeatus Zone (sample A25)

This zone corresponds to the former Middle *expansa* Zone and can be recognized by the first entry of *Bispathodus aculeatus aculeatus* Branson & Mehl, 1934a in level A25 which ranges from Middle *expansa* Zone (Ziegler & Sandberg, 1984)–*texanus* Zone (Lane et al., 1980). *Clydagnathus ormistoni* Beinert et al., 1971 becomes extinct in this conodont zone.

Bispathodus costatus Zones (sample A26)

The first appearance of *Bispathodus costatus* Branson, 1934 M1 (Ziegler and Sandberg 1984) is the indicator of the lower boundary of this interval. *Bispathodus bispathodus*, *Bispathodus spinulicostatus*, *Pseudopolygnathus* cf. *primus*, *Polygnathus communis collinsoni*, *Bispathodus jugosus*, *Palmatolepis gracilis expansa*, *Polygnathus perplexus* and *Bispathodus* cf. *costatus* are also present.

Bispathodus ultimus Zone (samples A27–A29)

This re-defined *Bispathodus ultimus* Zone is equivalent to the Upper *expansa* and *praesulcata* zones and the *costatus–kockeli* Interregnum of Kaiser et al. (2009). The lower limit of this zone is recognized by the first appearance of *Bispathodus ultimus* (Bischoff 1957 M1 and M2) which ranges from the Upper *expansa* Zone into the Middle *praesulcata* Zone (Ziegler and Sandberg 1984). The assemblage of *Bispathodus spinulicostatus*, *Pseudopolygnathus* cf. *primus*, *Bispathodus aculeatus aculateus*, *Polygnathus communis collinsoni*, *Bispathodus costatus*, *Bispathodus bispathodus* and *Palmatolepis gracilis expansa* was found in this interval.

According to the conodont zonation scheme proposed by Corradini et al. (2016) and Spalletta et al. (2017), the upper boundary is determined by the lower part of the FAD of *Protognathodus kockeli*, but due to the lack of *Protognathodus* and only one species of *Siphonodella praesulcata* in the Anarak section, there was no evidence for discrimination of the latest Famennian, *praesulcata*, the *costatus–kockeli* Interregnum (*ck*I) and *kockeli* conodont zones.

?*Protognathodus kockeli*–L. *Siphonodella crenulata* zones (samples A30–A32)

This interval falls within the first occurrence of red marly nodular limestone at the base of Shishtu Formation. The boundary between the grey limestone of the Bahram Formation and the overlying red nodular limestones of the Shishtu Formation is characterized by a sharp depositional contact. The lack of zonal conodont index species at the base of this interval prevents the identification of the Devonian/Carboniferous boundary. The rare conodont fauna with *Protognathodus collinsoni*, *Polygnathus inornatus*, *Polygnathus longiposticus* and *Polygnathus parapetus* (Fig. 7), comprised with *Siphonodella sulcata*–Lower *Siphonodella crenulata* zones. The lack of biostratigraphic data might be a result of a depositional hiatus which is related to the Hercynian orogeny. Wendt et al. (2005) also reported a discontinuity from the Anarak section around the same level.

Siphonodella isosticha–Upper *Siphonodella crenulata* to Upper *Gnathodus typicus* zones (samples A33–A35)

The entry of *Gnathodus delicatus*, *Gnathodus cueniformis*, *Gnathodus semiglaber* and *Gnathodus typicus* was observed in level 33. Due to the poorness of conodonts in that level, it is difficult to provide a precisely defined conodont zone; thus, only a stratigraphical range can be given.

Scaliognathus anchoralis–*Doliognathus latus* Zone (samples A36–A37)

The lower limit of this interval is recognized by the first appearance of *Gnathodus pseudosemiglaber* Thomson & Fellows, 1970 in level A35 which ranges from within the *anchoralis–latus* Zone through the *texanus* Zone (Lane et al. 1980; Belka and Korn 1994). The conodont assemblage is quite scarce, and only *Gnathodus semiglaber* and *Gnathodus typicus* Hass, 1953 have been recovered in this interval.

Upper *Gnathodus texanus* to *Adetognathus unicornis* zones (samples A38–A45)

The lower boundary of this zone, which is close to the base of the early Viséan, is marked by the FAD of *Locheria commutata* Branson & Mehl, 1941, and the second conodont found in this level is *Gnathodus bilineatus bilineatus* Roundy, 1926. Both taxa were recorded as index species of early Viséan (Meischner and Nemyrovska 1999; Nemyrovska et al. 2006; Sudar et al. 2018).

Rachistognathus muricatus Zone (samples A46–A48)

The first appearance of *Rhachistognathus muricatus* (Dunn 1966) in level A46 indicates the *Rachistognathus muricatus* Zone. This conodont zone is assigned to the late Serpukhovian just below the Mississippian/Pennsylvanian boundary. The upper boundary of the zone coincides with the first appearance of *Diclinognathodus noduliferus* s.l. (Ellison and Graves 1941), and *D. noduliferus* conodont Zone conformably lies above the *Rachistognathus muricatus* Zone. The range of this species is from Upper Mississippian to Lower Pennsylvanian (Krumhardt et al. 1996). *Gnathodus girtyi girtyi* and *Gnathodus girtyi simplex* are the other species which occur in this interval (Fig. 7).

Serpukhovian–Bashkirian (mid-Carboniferous) Boundary

Many conodont specialists indicate that the common early Carboniferous genera *Gnathodus*, *Lochriea* and *Cavusgnathus* become extinct at the end of Serpukhovian, and the first Bashkirian *Declinognathodus* appeared at the mid-Carboniferous boundary between Mississippian and Pennsylvanian (Brenckle et al. 1997; Lane et al. 1999; Nemirovskaya 1999; Richards and Aretz 2010; Krumhardt et al. 1996). In 1995, International Subcommission on Carboniferous Stratigraphy selected the Arrow Canyon, Nevada (USA), to be the GSSP for the mid-Carboniferous boundary. The first appearances of the index conodont taxon *Declinognathodus noduliferus* sensu lato, including the subspecies *Declinognathodus noduliferus noduliferus*, *Declinognathodus noduliferus inaequalis* and *Declinognathodus noduliferus japonicus*, were approved as the biostratigraphic marker for the mid-Carboniferous boundary (Baesemann and Lane 1985; Nemirovskaya and Nigmadganov 1994; Nemyrovskaya 1999; Lane et al. 1999; Gradstein et al. 2004; Özdemir 2012).

Declinognathodus noduliferus (samples A49–A51)

The lower limit of this interval is recognized by the first appearance of *D. noduliferus* s.l. Ellison and Graves, 1941 in level 49, 108 m above the base of studied section. Conodonts from the level between 108 and 135 m above the base of the section are *D. noduliferus* and *Declinognathodus*

praenoduliferus Nigmadganov and Nemirovskaya 1992. In original definition of *Declinognathodus praenoduliferus*, it appears earlier than *D. noduliferus* s.l., but in Iranian sections, both species have the same range starting from the *Eumorphoceras–Homoceras* boundary and in the *D. noduliferus* conodont Zone. The last occurrence of *D. noduliferus* s.l. at 135 m above the base indicates the upper boundary of *D. noduliferus* Zone which is conformably overlain by the *Idiognathoides sinuatus–Rachistognathus minutus* Zone. The upper limit also can be identified by the first presence of *Rachistognathus minutus minutus* (Higgins and Bouckaert 1968) in level A51 at the base of next interval.

Idiognathoides sinuatus–Rachistognathus minutus Zone (samples A51–A53)

Conodonts collected from samples A51, A52 and A53 at 135 m from the base of section contained *Rachistognathus minutus minutus* (Higgins and Bouckaert 1968). The range of this species is lower Morrowan (base of *sinuatus–minutus* Zone) in North America (Varker et al. 1991). This interval falls within the first occurrence of thick-bedded micritic limestone which is characterized by a sharp boundary to the lower brecciated limestone. The *I. sinuatus–R. minutus* Zone belongs to the middle Bashkirian and defines the upper boundary of *D. noduliferus* Zone. *Declinognathodus noduliferus* and *Declinognathodus praenoduliferus* are also present in this interval.

Conclusions

Late Palaeozoic Upper Devonian to Lower Carboniferous rocks in Central Iran exhibit a number of different lithologies, which point to a shallow-water shelf setting (Bahrami et al. 2018, 2019; Königshof et al. 2017). Several hiatuses exist due to lateral facies changes and/or synsedimentary vertical movements in the late Palaeozoic which is associated with horst-and-graben structures in different tectonic blocks. The late Palaeozoic (Late Devonian–Permian) deposits of the Anarak section suggest widespread marine conditions. The gradual transition and lithologic similarities between Devonian and Lower Carboniferous (Mississippian) shows that the depositional regime remained virtually unchanged. On the other hand, many sections in Iran exhibit biostratigraphical hiatuses or facies changes, which particularly concern the conodont record (e.g. Königshof et al. in press). However, some section exhibits a rather complete succession, such as the Anarak section. Sediments of this section range from the Middle Devonian and Frasnian (see Bahrami et al. 2019) to the Late Devonian and Mississippian/Pennsylvanian boundary.

University of Isfahan in cooperation with the Senckenberg Research Institute and Natural History Museum, Frankfurt. We thank Jeffrey Over (USA) and an anonymous reviewer for their critical comments which improved an earlier version of the manuscript. This is a contribution to the International Geological Science Programmes IGCP 652 and IGCP 700.

Compliance with ethical standards

Conflict of interest The authors declare that they have no conflict of interest.

References

Aghanabati, A. (2010). Stratigraphy of Iran. Geological Survey of Iran, Tehran, 1297 p.

Almasian, M. (1997). Tectonics of the Anarak area (Central Iran). Ph.D. thesis, *University of Islamic Azad, Science and Research Unit*, 164 p.

Ariuntogos, M., Königshof, P., Hartenfels, S., Jansen, U., Nazik, A., Carmichael, S.K., Waters, J.A., Sersmaa, G., Crônier, C., Ariunchimeg, Ya, Pascall, O., & Dombrowski, A. (in press). The Hushoot Shiveetiin gol section (Baruunhuurai Terrane): sedimentology and facies from a Late Devonian island arc setting. *Palaeobiodiversity and Palaeoenvironments* (in press).

Baesemann, J. F., & Lane, H. R. (1985). Taxonomy and evolution of the genus *Rhachistognathus* Dunn (conodonts; late Mississippian to early middle Pennsylvanian). *Courier Forschungsinstitut Senckenberg, 74*, 93–136.

Bagheri, S., & Stampfli, G. (2008). The Anarak, Jandaq and Posht-e-Badam metamorphic complexes in Central Iran: new geological data, relationships and tectonic implications. *Tectonophysics, 451*, 123–155.

Bahrami, A., Boncheva, I., Königshof, P., Yazdi, M., & Ebrahimi Khan Abadi, A. (2014). Conodonts of Mississippian/Pennsylvanian boundary interval in Central Iran. *Journal of Asian Earth Science, 92*, 187–200.

Bahrami, A., Königshof, P., Boncheva, I., Yazdi, M., Ahmadi Nahre Khalaji, M., & Zarei, E. (2018). Conodont biostratigraphy of the Kesheh and Dizlu sections, and the age range of the Bahram Formation in Central Iran. *Palaeobiodiversity and Palaeoenvironments, 98*, 315–329.

Bahrami, A., Königshof, P., Vaziri-Moghaddam, H., Shakeri, B., & Boncheva, I. (2019). Conodont stratigraphy and conodont biofacies of the shallow-water Kuh-e-Bande-Abdol-Hossein section (SE Anarak, Central Iran). *Palaeobiodiversity and Palaeoenvironments, 99*, 477–494.

Bakhtiari, S. (2005). Road atlas of Iran Gitashenasi. *Geological and Cartographic Institute, 1*, 1,000,000 Tehran, Iran.

Beinert, R. J., Klapper, G., Sandberg, C. A., & Ziegler, W. (1971). Revision of Scaphignathus and description of Clydagnathus? ormistoni n. sp. (Conodonta, Upper Devonian). *Geologica et Palaeontologica, 5*, 81–91.

Belka, Z., & Korn, D. (1994). Re-evaluation of the Early Carboniferous conodont succession in the Esla area of the Cantabrian Zone (Cantabrian Mountains, Spain). *Courier Forschungsinstitut Senckenberg, 168*, 183–193.

Berberian, F., & King, G. C. P. (1981). Towards a paleogeography and tectonic evolution of Iran. *Canadian Journal of Earth Science, 5*, 101–117.

Bischoff, G. (1957). Die Conodonten-Stratigraphie des rhenoherzynischen Unterkarbons mit Berücksichtigung der Wocklumeria-Stufe und der Devon/KarbonGrenze. *Abhandlungen Hessisches Landesamt für Bodenforschung, 19*, 1–64.

Bischoff, J. W., Montanez, I. P., Gulbranson, E. L., & Brenckle, P. L. (2009). The onset of mid-Carboniferous glacio-eustasy: sedimentologic and diagenetic constraints, Arrow Canyon, Nevada. *Palaeogeography, Palaeoclimatology Palaeoecology, 276*, 217–243.

Bischoff, J. W., Montanez, I. P., & Osleger, D. A. (2010). Dynamic Carboniferous climate change, Arrow Canyon, Nevada. *Geosphere, 6*(1), 1–34.

Boncheva, I., Bahrami, A., Yazdi, M., & Toraby, H. (2007). Carboniferous Conodont biostratigraphy and late Paleozoic platform evolution in south Central Iran (Asadabad section in Ramsheh area - SE Isfahan). *Rivista Italiana di Paleontologiae Stratigrafa, 113*(3), 329–356.

Branson, E. R. (1934). Conodonts from the Hannibal Formation of Missouri. *Missouri University Studies, 8*, 301–343.

Branson, E. B., & Mehl, M. G. (1934a). Conodonts from the Grassy Creek shale of Missouri. *Missouri University Studies, 8*, 171–259.

Branson, E. B., & Mehl, M. G. (1934b). Conodonts from the Bushberg sandstone and equivalent formations of Missouri. *Missouri University Studies, 4*, 265–300.

Brenckle, P.L., Baesemann, J.F., Lane, H.R., West, R.R., Webster, G., Langenheim, R.L., Brand, U., & Richards, B.C. (1997). Arrow Canyon, the Mid-Carboniferous boundary stratotype. In P.L. Brenckle and W.R. Page, (eds.), *Paleoforams '97 guidebook: postconferrence field trip to the Arrow Canyon Range, Southern Nevada, U.S.A.* Cushman Foundation for Foraminiferal Research Supplement to Special Publication 36, 13–32.

Brezinski, D. K., Cecil, C. B., Skema, V. W., & Stamm, R. (2008). Late Devonian glacial deposits from the eastern United States signal an end of the mid-Paleozoic warm period. *Palaeogeography, Palaeoclimatology, Palaeoecology, 268*, 143–151.

Brezinski, D. K., Cecil, C. B., & Skema, V. W. (2010). Late Devonian glaciogenic and associated facies from the central Appalachian Basin, Eastern United States. *Geological Society of America Bulletin, 122*, 265–281.

Buggisch, W., Joachimski, M. M., Sevastopulo, G., & Morrow, J. (2008). Mississippian $\delta^{13C carb}$ and conodont apatite δ^{18O} records? Their relation to the late Palaeozoic glaciation. *Palaeogeography, Palaeoclimatology, Palaeoecology, 268*, 273–292.

Bultynck, P. (2003). Devonian Icriodontidae: biostratigraphy, classification and remarks on paleoecology and dispersal. *Revista Espanola de Micropaleontologia, 35*(3), 295–314.

Caplan, M. L., & Bustin, R. M. (1999). Devonian-Carboniferous Hangenberg mass extinction event, widespread organic-rich mudrock and anoxia: causes and consequences. *Palaeogeography, Palaeoclimatology, Palaeoecology, 148*, 187–207.

Caplan, M. L., Bustin, R. M., & Grimm, K. A. (1996). Demise of a Devonian-Carboniferous carbonate ramp by eutrophication. *Geology, 24*(8), 715–718.

Caputo, M. V. (1985). Late Devonian glaciation in South America. *Palaeogeography, Palaeoclimatology, Palaeoecology, 51*, 291–317.

Caputo, M.V., Melo, J.H.G., Streel, M., & Isbell, J.L. (2008). Late Devonian and Early Carboniferous glacial records of South America. In: Fielding, C.R., Frank, T.D., Isbell, J.L. (eds.), *Resolving the late Paleozoic ice age in time and spa*ce. Geological Society of America, special papers 441, 161–173.

Carmichael, S., Waters, J., Königshof, P., Suttner, T., & Kido, E. (2019). Paleogeography and paleoenvironments of the Late Devonian Kellwasser Event: a review of its sedimentological and geochemical expression. *Global and Planetary Change, 183*, 102984. https://doi.org/10.1016/j.gloplacha.2019.102984.

Cooper, C. L. (1939). Conodonts from a Bushberg-Hannibal horizon in Oklahoma. *Journal of Paleontology, 13*, 379–422.

Corradini, C., Spalletta, C., Mossoni, A., Matyja, H., & Over, D. J. (2016). Conodont across the Devonian/Carboniferous boundary: a review and implication for the redefinition of the boundary and a proposal for an updated conodont zonation. *Geological Magazine*, 1–15.

Davoudzadeh, M., Soffel, H., & Schmidt, K. (1981). On the rotation of the Central-East-Iran microplate. *Neues Jahrbuch für Geologie und Paläontologie, 3*, 180–192.

Druce, E. C. (1969). Devonian and Carboniferous conodonts from Bonaparte Gulf Basin, Northen Australia. *Bureau of Mineral Resources, Geology and Geophysics Bulletin, 69*, 1–243.

Dunn, D. L. (1966). New Pennsylvanian platform conodonts from Southwestern United States. *Journal of Paleontology, 40*, 1294–1303.

Dzik, J. (2006). The Famennian "Golden Age" of conodonts and ammonoids in the Polish part of the Variscan Sea. *Palaeontologia Polonica, 63*, 1–359.

Ellison, S. P., & Graves Jr., R. W. (1941). Lower Pennsylvanian (dimple limestone) conodonts of the Marathon region, Texas. *Journal of Paleontology, 14*, 21.

Epstein, A. G., Epstein, J. B., & Harris, L.D. (1977). Conodont color alteration - an index to organic metamorphism. *U.S. Geological Survey Professional Paper, 995*, 1–27.

Garzanti, E., & Sciunnach, D. (1997). Early Carboniferous onset of Gondwanian glaciation and Neo-tethyan rifting in South Tibet. *Earth and Planetary Science Letter, 148*, 359–365.

Girard, C., Klapper, G., & Feist, R. (2005). Subdivision of the terminal Frasnian linguiformis conodont Zone, revision of the correlative interval of Montagne Noire Zone 13, and discussion of stratigraphically significant associated trilobites. In D. J. Over, J. R. Morrow, & P. B. Wignall (Eds.), *Understanding Late Devonian and Permian-Triassic biotic and climatic events: towards an integrated approach*, *Developments in Palaeontology and Stratigraphy 20* (pp. 181–198). Amsterdam: Elsevier.

Gradstein, F.M., J. G., Ogg, A.G., Smith, F.P., Agterberg, W., Bleeker, R.A., Cooper, V., Davydov, P., Gibbard, L.A., Hinnov, M.R., House, L., Lourens, H-P., Luterbacher, J., McArthur, M.J, Melchin, L.J., Robb, P.M., Sadler, J., Shergold, M., Villeneuve, B.R., Wardlaw, J., Ali, H., Brinkhuis, F.J., Hilgen, J., Hooker, R.J., Howarth, A.H., Knoll, J., Laskar, S., Monechi, J, Powell, K.A., Plumb, I., Raffi, U., Röhl, A., Sanfilippo, B., Schmitz, N.J., Shackleton, G.A, Shields, H., Strauss, J., Van Dam, J., Veizer, TH., Van Kolfschoten, & Wilson, D. (2004) Geologic time scale 2004. Cambridge University Press, 589 pp.

Hairapetian, V., Korn, D., & Bahrami, A. (2006). Viséan and Bashkirian ammonoids from Central Iran. *Acta Geologica Polonica, 56*(3), 229–240.

Hairapetian, V., Ghobadipour, M., Popov, L. E., Hejazi, S. H., & Holmer, L. E. (2015). Ordovician of the Anarak region: implications in understanding early Palaeozoic history of Central Iran. *Stratigraphy, 12*(2), 22–30.

Hartenfels, S. (2011). Die globalen Annulata-Events und die Dasberg-Krise (Famennium, Oberdevon) in Europa und Nord-Afrika: hochauflösende Conodonten-Stratigraphie, Karbonat-Mikrofazies, Paläoökologie und Paläodiversität. *Münstersche Forschungen zur Geologie und Paläontologie, 105*, 17–527.

Hashemie, A., Rostamnejad, A., Nikbakht, F., Ghorbanie, M., Rezaie, P., & Gholamalian, H. (2015). Depositional environments and sequence stratigraphy of the Bahram Formation (middle-late Devonian) in north of Kerman, South-Central Iran. *Geoscience Frontiers, 7*, 821–834.

Hass, W. H. (1953). Conodonts of the Barnett Formation of Texas. *U.S. Geol. Survey Prof. Paper, 243F*, 69–94.

Heim, N. A. (2009). Stability of regional brachiopod diversity structure across the Mississippian/Pennsylvanian boundary. *Paleobiology, 35*(3), 393–412.

Helms, J. (1959). Conodonten aus dem Saalfelder Oberdevon (Thüringen). *Geologie, 8*, 634–677.

Helms, J. (1961). Die "nodocostata-Gruppe" der Gattung Polygnathus. *Geologie, 10*(6), 674–711.

Helms, J. (1963). Zur Phylogenese und Taxonomie von Palmatolepis (Conodontida, Oberdevon). *Geologie, 12*(4), 449–485.

Higgins, A.C., Bouckaert, J. (1968). Conodont stratigraphy and paleontology of the Namurian of Belgium. *Memoir du Service Geologique de Belgique* 10, 64 pp.

Huang, C., & Gong, Y. M. (2016). Timing and patterns of the Frasnian–Famennian event: evidences from high-resolution conodont biostratigraphy and event stratigraphy. *Palaeogeography and Palaeoecolgy, 448*, 317–338.

Huckriede R., Kürsten M. & Venzlaff H. (1962). Zur Geologie des Gebietes zwischen Kerman und Saghand (Iran). *Beihefte zum Geologischen Jahrbuch 51*, 197 pp.

Huddle, J. W. (1934). Conodonts from the New Albany Shale of Indiana. *Bulletin America Paleontology, 21*, 1–136.

Husseini, M. I. (1991). Tectonic and depositional model of the Arabian and adjoining plates during the Silurian-Devonian. *American Association of Petroleum Geologists Bulletin, 75*, 108–120.

Isaacson, P. E., Hladil, J., Shen, J. W., Kalvoda, J., & Grader, G. (1999). Late Devonian (Famennian) glaciation in South America and marine offlap on other continents. *Abhandlungen der Geologischen Bundesanstalt, 54*, 239–257.

Isaacson, P. E., Diaz-Martinez, E., Grader, G. W., Kalvoda, J., Babek, O., & Devuyst, F. X. (2008). Late Devonian–earliest Mississippian glaciation in Gondwanaland and its biogeographic consequences. *Palaeogeography, Palaeoclimatology, Palaeoecology, 268*, 126–142.

Isbell, J.L., Cole, D.I., & Catuneanu, O. (2008a). Carboniferous-Permian glaciation in the main Karoo Basin, South Africa: stratigraphy, depositional controls, and glacial dynamics. In C.R. Fielding (Ed.). Resolving the late Paleozoic ice age in time and space. *Geological Society of America Special Paper, 441*, 71–82.

Isbell, J.L., Kosch, Z.J., Szablewski, G.M., Lenaker, P.A. (2008b). Permian glacigenic deposits in the Transantarctic Mountains, Antarctica. In C.R. Fielding. (Ed.). Resolving the late Paleozoic ice age in time and space. *Geological Society of America Special Paper, 441*, 59–70.

Jeppsson, L., & Anehus, R. (1995). A buffered formic acid technique for conodont extraction. *Journal of Paleontology, 69*(4), 790–794.

Ji, Q., & Ziegler, W. (1993). The Lali section: an excellent reference section for Late Devonian in South China. *Courier Forschungs-Institut Senckenberg, 157*, 1–183.

Joachimski, M. M., & Buggisch, W. (2002). Conodont apatite δ18O signatures indicate climatic cooling as a trigger of the Late Devonian (F-F) mass extinction. *Geology, 30,* 711–714.

Joachimski, M. M., van Geldern, R., Breisig, S., Day, J., & Buggisch, W. (2004). Oxygen isotope evolution of biogenic calcite and apatite

during the Middle and Upper Devonian. *International Journal of Earth Science, 93*, 542–553.

Joachimski, M. M., von Bitter, P. H., & Buggisch, W. (2006). Constraints on Pennsylvanian glacioeustatic sea-level changes using oxygen isotopes of conodont apatite. *Geology, 34*(4), 277–280.

Kaiser, K., Miehe, G., Schoch, W. H., Zander, A., & Schlütz, F. (2006). Edogeomorphology, geochronology and paleobotany of soil profiles obtained in the Kyichu River catchment, southern Tibet. *Pangaea*. https://doi.org/10.1594/PANGAEA.787121.

Kaiser, S. I., Becker, R. T., Spalletta, C., & Steuber, T. (2009). High-resolution conodont stratigraphy, biofacies and extinctions around the Hangenberg event in pelagic successions from Austria, Italy and France. *Palaeontographica Americana, 63*, 97–139.

Kaiser, S. I., Becker, R. T., Steuber, T., & Aboussalam, Z. S. (2011). Climate-controlled mass extinctions, facies, and sea-level changes around the Devonian-Carboniferous boundary in the eastern Anti-Atlas (SE Morocco). *Palaeogeography, Palaeoclimatology, Palaeoecology, 310*, 340–364.

Kaiser, S. I., Aretz, M., & Becker, R. T. (2016). The global Hangenberg Crisis (Devonian–Carboniferous transition): review of a first-order mass extinction. *Geological Society of London Special Publication, 423*, 387–437.

Kammer, T. W., & Ausich, W. I. (2006). The Bage of crinoids: a Mississippian biodiversity spike coincident with widespread carbonate ramps. *Palaios, 21*, 238–248.

Klapper, G. (1958). An Upper Devonian conodont fauna from the Darby Formation of the Wind River Mountains, Wyoming. *Journal of Paleontology, 32*, 1082–1093.

Klapper, G., & Lane, H. R. (1985). Upper Devonian (Frasnian) conodonts of the Polygnathus biofacies, N.W.T., Canada. *Journal of Paleontology, 59*, 904–951.

Klapper, G. & Ziegler, W. (1979). Devonian conodont biostratigraphy. In M.R. House, C.T. Scrutton, & M.G. Bassett, (Eds.), The Devonian system. *Special Papers in Paleontology, 23*, 199-224.

Königshof, P., Bahrami, A., & Kaiser, S.I. (in press). Devonian-Carboniferous boundary sections in Iran. In M. Aretz, & C. Corradini (eds.) Global review of the Devonian-Carboniferous Boundary. Palaeobiodiversity and Palaeoenvironments (in press). https://doi.org/10.1007/s12549-020-00438-z

Königshof, P., Carmichael, S., Waters, J., Jansen, U., Bahrami, A., Boncheva, I. & Yazdi, M. (2017). Palaeoenvironmental study of the Palaeotethys Ocean: The Givetian/Frasnian boundary of a shallow-marine environment using combined facies analysis and geochemistry (Zefreh Section/Central Iran). In B. Mottequin, L. Slavik & P. Königshof (eds.) Climate change and biodiversity patterns in the mid-Palaeozoic – Proceedings-Volume IGCP 596/SDS Meeting Brussels (2015). *Palaeobiodiversity and Palaeoenvironments, 97*(3), 517–540. https://doi.org/10.1007/s12549-016-0253-0.

Korn, D., Kaufmann, B., Wendt, J., & Karimi Bavandpur, A. R. (1999). Carboniferous ammonoids from Anarak (Central Iran). *Abhandlungen Geologischen Bundesanstalt, 54*, 337–344.

Krumhardt, A. P., Harris, A., & Watts, K. F. (1996). Lithostratigraphy, microlithofacies, and conodont biostratigraphy and biofacies of the Wahoo limestone (Carboniferous), Eastern Sadlerochit Mountains, Northeast Brooks Range, Alaska. *United States Geological Survey Professional Paper, 1568*, 1–70.

Kumpan, T., Bábek, O., Kalvoda, J., Frýda, J., & Matys Grygar, T. (2014a). A high-resolution, multiproxy stratigraphic analysis of the Devonian–Carboniferous boundary sections in the Moravian Karst (Czech Republic) and a correlation with the Carnic Alps (Austria). *Geological Magazine, 151*, 201–215.

Kumpan, T., Bábek, O., Kalvoda, J., Matys Grygar, T., & Frýda, J. (2014b). Sea-level and environmental changes around the Devonian–Carboniferous boundary in the Namur–Dinant Basin (S Belgium, NE France): a multi- proxy stratigraphic analysis of

carbonate ramp archives and its use in regional and interregional correlations. *Sedimentary Geology, 311*, 43–59.

Kuzmin, A. V., & Melnikova, L. I. (1991). Novyye rannefamenskiye konodonty. *Paleontological Zhurnal, 25*, 120–125.

Lakin, J. A., Marshall, J. E. A., Troth, I., & Harding, I. C. (2016). Greenhouse to icehouse: a biostratigraphic review of latest Devonian–Mississippian glaciations and their global effects. In R. T. Becker, P. Königshof, & C. E. Brett (Eds.), *Devonian climate, sea level and evolutionary events*. *London*, Special Publications, 423. First published online April 15, 2016: *Geological Society*. https://doi.org/10.1144/SP423.12.

Lane, H. R., Sandberg, C., & Ziegler, W. (1980). Taxonomy and phylogeny of some Lower Carboniferous conodonts and preliminary standard post – Siphonodella zonation. *Geologica et Paläontologica, 14*, 117–164.

Lane, H. R., Brenckle, P. L., Baesemann, J. F., & Richards, B. C. (1999). The IUGS boundary in the middle of the Carboniferous: arrow Canyon Nevada, USA. *Episodes, 22*, 272–283.

Lensch, G., & Davoudzadeh, M. (1982). Ophiolites in Iran. *Neues Jahrbuch für Geologie und Paläontologie Monatshefte*, 306–320.

Leven, E. J., & Gorgij, M. N. (2009). Section of Permian deposits and Fusulinids in the Halvan Mountains, Yazd Province, Central Iran. *Stratigrafiya Geologicheskaya Korrelyatsiya, 17*, 49–67.

Leven, E. J., Davydov, V. I., & Gorgij, M. N. (2006). Pennsylvanian stratigraphy and fusulinids of Central and Eastern Iran. *Palaeontologica Electronica, 9*, 1–36.

López-Gamundi, O. R. (1997). Glacial–postglacial transition in the late Palaeozoic basins of South America. In I. P. Martini (Ed.), *Late glacial and postglacial environmental changes—Quarternary, Carboniferous–Permian, and Proterozoic* (pp. 147–168). New York: Oxford University Press.

López-Gamundi, O. R., & Martínez, M. (2000). Evidence of glacial abrasion in the Calingasta–Uspallata and western Paganzo basins, mid-Carboniferous of western Argentina. *Palaeogeography, Palaeoclimatology, Palaeoecology, 159*, 145–165.

Lowry, D. P., Poulsen, C. J., Horton, D. E., Torsvik, T. H., & Pollard, D. (2014). Thresholds for Paleozoic ice sheet initiation. *Geology, 42*, 627–630. https://doi.org/10.1130/G35615.1.

Marynowski, L., Zatoń, M., Rakociński, M., Filipiak, P., Kurkiewicz, S., & Pearce, T. J. (2012). Deciphering the upper Famennian Hangenberg Black Shale depositional environments based on multi-proxy record. *Palaeogeography, Palaeoclimatology, Palaeoecology, 346*(347), 66–86.

Mehl, M. G., & Thomas, L. A. (1947). Conodonts from the Fern Glen of Missouri. *Journal of Science Laboratory of Denison University, 40*, 3–20.

Meischner, D., & Nemyrovska, T. (1999). Origin of Gnathodus bilineatus (Roundy, 1926) related to goniatite zonation in Rhenisches Schiefergebirge, Germany. *Bolletino Della Società Paleontologica Italiana, 37*, 427–442.

Metzger, R. A. (1994). Multielement reconstructions of Palmatolepis and Polygnathus (Upper Devonian, Famennian) from the Canning Basin, Australia, and Bactrian Mountain, Nevada. *Journal of Paleontology, 68*(3), 617–647. https://doi.org/10.1017/S0022336000025956.

Montanez, I. P., Tabor, N. J., Niemeier, D., DiMichele, W. A., Frank, T. D., Fielding, C. R., Isbell, J. L., Birgenheier, L. P., & Rygel, M. C. (2007). Vegetation instability during late Paleozoic deglaciation. *Science, 315*, 87–91.

Müller, K. J. (1956). Zur Kenntnis der Conodonten-Fauna des europaischen Devons, 1; Die Gattung Palmatolepis. *Abhandlunghen and Senckenbergischen Naturforschenden Gesellschaft, 494*, 1–70.

Mullins, G. L., & Servais, T. (2008). The diversity of the Carboniferous phytoplankton. *Review of Palaeobotany and Palynology, 149*, 29–49. https://doi.org/10.1016/j.revpalbo.2007.10.002.

Muttoni, M., Mattei, M., Balini, A., Zanchi, M., Gaetani, M., & Berra, F. (2009) The drift history of Iran from the Ordovician to the Triassic. In: M.-F., Brunet, M., Wilmsen & J.W., Granath (eds.). *South Caspian to Central Iran basins*. Geological Society London Special Publication 312, 7–29.

Nemirovskaya, T. I. (1999). *Bashkirian Conodonts of the Donets Basin* (115 p). Scripta Geologica: Ukraine.

Nemirovskaya, T. I., & Nigmadganov, I. M. (1994). The Mid-Carboniferous conodont event. *Courier Forschungsinstitut Senckenberg, 168*, 319–333.

Nemyrovska, T. I., Perret-Mirouse, M.-F., & Weyant, M. (2006). The early Viséan (Carboniferous) conodonts from the Saoura Valley, Algeria. *Acta Geologica Polonica, 56*, 361–370.

Nigmadganov, I. M., & Nemirovskaya, T. I. (1992). Mid-Carboniferous boundary conodonts from the Gissar ridge, South Tienshan, Middle Asia. *Courier Forschungsinstitut Senckenberg, 154*, 253–275.

Ovanatanova, N. S. (1969). New Upper Devonian conodonts from the central region of the Russian platform and of the Timan: In Fauna and stratigraphy of the Palaeozoic of the Russian platform. *Nedra*, 39–141.

Ovnatanova, N. S., & Kononova, L. I. (2001). Conodonts and Upper Devonian (Frasnian) biostratigraphy of central regions of Russian platform. *Courier Forschungsinstitut Senckenberg, 233* 115 p.

Ovnatanova, N. S., & Kononova, L. I. (2008). Frasnian conodonts from the Eastern Russian Platform. *Paleontological Journal, 42*(10), 997–1166.

Özdemir, A. (2012). Stage boundries in the Mississippian of Taurides based on conodont data: statistical analysis taxonomy and biostatigraphy. PhD thesis, *The Graduate School of Natural and Applied Science of Middle East Technical University*, 358p.

Paschall, O., Carmichael, S. K., Königshof, P., Waters, J. A., Ta, P. H., Komatsu, T., & Dombrowski, A. (2019). The Devonian-Carboniferous boundary in Vietnam: sustainedocean anoxia with a volcanic trigger for the Hangenberg Crisis? *Global and Planetary Change, 175*, 64–81.

Perri, M. C., & Spalletta, C. (1990). Famennian conodonts from climenid pelagic limestone, Carnic Alps, Italy. *Palaeontographia Italica, 77*, 55–83.

Powell, M. G. (2005). Climatic basis for sluggish macroevolution during the late Paleozoic ice age. *Geology, 33*, 381–384.

Powell, M. G. (2007). Latitudinal diversity gradients for brachiopod genera during late Palaeozoic time: links between climate, biogeography and evolutionary rates. *Global Ecology Biogeography, 16*, 519–528.

Richards, B. C., & Aretz, M. (2010). Report on the SCCS field meeting in the Cantabrian Mountains, Northwest Spain, June 4th-10th, 2010. *Newsletter on Carboniferous Stratigraphy, 28*, 7–14.

Roudny, P.V. (1926). Part 2. The micro-fauna, in Roundy, P. V., Girty, G. H., and Goldman, M. I., Mississippian formations of San Saba County, Texas. U. S. Geological Survey Prof. Paper 146, 5–23.

Ruttner, A., & Stöcklin, J. (1966). Forward, with key map, stratigraphy summary and description of fossil localities. *Geology of the Shirgesht area, 6*, 2–6.

Ruttner, A., Nabavi, M., & Hajian, J. (1968). Geology of the Shirgesht area (Tabas area, East Iran). *Geological Survey Iran Rep, 4*, 1–133.

Sandberg, C.A. & Dreesen, R. (1984). Late Devonian icriodontid biofacies models and alternate shallow water conodont zonation, 143–178. In Clark, D.L. (ed.) Conodont biofacies and provincialism. *Geological Society of America Special Paper, 196*. https://doi.org/10.1130/SPE196-p143.

Sandberg, C. A., & Ziegler, W. (1973). Refinement of standard Upper Devonian conodont zonation based on sections in Nevada and West Germany. *Geologica et Palaeontologica, 7*, 97–122.

Sandberg, C. A., & Ziegler, W. (1979). Taxonomy and biofacies of important conodonts of Late Devonian styriacus-Zone, United States and Germany. *Geologica et Palaeontologica, 13*, 173–212.

Sannemann, D. (1955a). Oberdevonische Conodonten (to II). *Senckenbergiana Lethaea, 36*, 123–156.

Sannemann, D. (1955b). Beitrag zur Untergliederung des Oberdevons nach Conodonten. *Neues Jahrbuch für Geologie und Paläontologie, Abhandlungen, 100*, 324–331.

Sardar Abadi, M., Kulagina, E., Voeten, D. F. A. E., Boulvain, F., & Da Silva, A. C. (2017). Sedimentologic and paleoclimatologic reconstructions of carbonate factory evolution in the Alborz Basin (Northern Iran) indicate a global response to Early Carboniferous (Tournaisian) glaciations. *Sedimentary Geology, 348*, 19–36.

Savag, N. M., & Funai, C. A. (1980). Devonian conodonts of probable Early Frasnian Age from the Coronados Islands of Southeastern Alaska. *Journal of Paleontology, 54*, 806–813.

Schallreuter, R., Hinz-Schallereuter, I., Balini, M., & Ferretti, A. (2006). Late Ordovician Ostracoda from Iran and their significance for palaeogeographical reconstructions. *Zeitschrift für Geologische Wissenschaften, 34*(5–6), 293–345.

Shakeri, B. (2017). Biostratigraphy of the Late Devonian deposits in Kuh-e-Bande-Abdol-Hossein (SE Anarak) section based on conodont fauna. MSc. thesis, University of Isfahan, 242 p.

Sharkovski, M., Susov, M., & Krivyakin, M. (1984). Geology of the Anarak area (Central Iran), explanatory text of the Anarak quadrangle map. *Geological Survey of Iran*, Scale, 1: 250. 000, V/O Technoexport, Report, 19. Tehran, 143 p.

Sharland, P. R., Archer, R., Casey, D. M., Davies, R. B., Hall, S. H., Heward, A. P., Horbury, A. D., & Simmons, M. D. (2001). Arabian plate sequence stratigraphy. In *GeoArabia special publication, 2*. Gulf PetroLink: Bahrain 371 p.

Soffel, H. C., Davoudzadeh, M., Rolf, C., & Schmidt, S. (1996). New palaeomagnetic data from Central Iran and a Triassic palaeo reconstruction. *Geologische Rundschau, 85*, 293–302.

Soreghan, G. S., & Giles, K. A. (1999). Amplitudes of late Pennsylvanian glacioeustasy. *Geology, 27*, 255–258.

Spalletta, C., Perri, M. C., Over, J., & Corradini, C. (2017). Famennian (Upper Devonian) conodont zonation: revised global standard. *Bulletin of Geosciences, 92*, 31–57.

Stauffer, C. R. (1938). Conodonts of the Olentangy Shale. *Journal of Paleontology, 12*, 41–433.

Stepanov. D.L. (1971). Carboniferous stratigraphy of Iran. In: VI Congress International Stratigraphie Géologique Carbonifère, Sheffield, 4, 1505–1518.

Stöcklin, J. (1968). Structural history and tectonic of Iran: a review. *American Association of Petroleum Geologists Bulletin, 52*, 1229–1258.

Stöcklin, J. (1971). *Stratigraphic lexicon of Iran part 1: Central, North and East Iran*. Tehran: Geological Survey of Iran 338 p.

Stöcklin, J., Eftekhar-Nezhad, J., & Hushmand-Zadeh, A. (1965). Reprinted, 1991. Geology of the Shotori Range (Tabas area, East Iran). *Geological Survey of Iran, Reports, 3*, 1–69.

Streel, M., Caputo, M. V., Loboziak, S., & Melo, J. H. G. (2000). Late Frasnian-Famennian climates based on palynomorph analyses and he question of the Late Devonian glaciations. *Earth Science Reviews, 52*, 121–173.

Streel, M., Caputo, M. V., Loboziak, S., Melo, J. H. G., & Thorez, J. (2001). Palynology and sedimentology of laminites and tillites from the latest Famennian of the Parnaíba Basin, Brazil. *Geologica Belgica, 3*, 87–96.

Sudar, M. N., Novak, M., Korn, D., & Jovanović, D. (2018). Conodont biostratigraphy and carbonate microfacies of the Late Devonian to Mississippian Milivojevića Kamenjar section (Družetić, NW Serbia). *Bulletin of Geosciences, 93*(2), 163–183.

Thomas, L. A. (1949). Devonian-Mississippian formations of Southeast Iowa. *Bulletin of the Geological Society of America, 60*, 403–138.

Thompson, T. L., & Fellows, L. D. (1970). Stratigraphy and Conodont biostratigraphy of Kinderhookian and Osagean (lower

Mississippian) rocks of southwestern Missouri and adjacent areas. *Missouri Geological Survey and Water Ressources, 45*, 1–263.

Ulrich, E. O., & Bassler, R. S. (1926). A classification of the toothlike fossils, conodonts, with descriptions of American Devonian and Mississippian species. *U.S. Natural History Museum, Proceedings, 68(12)* 63 P.

Varker, W.J., Owens, B., & Riley, N.J. (1991). Integrated biostratigraphy for the proposed mid-Carboniferous boundary stratotype, Stonehead Beck, Cowling, north Yorkshire, England, p. 79–84. In P. L. Brenckle and W. L. Manger (eds.), International correlation and division of the Carboniferous system. *Courier Forschungsinstitut Senckenberg* 130, 221–235.

Veevers, J. J., & Powell, C. M. (1987). Late Paleozoic glacial episodes in Gondwanaland reflected in transgressive-regressive depositional sequences in Euramerica. *Geological Society America Bulletin, 98*, 475–487.

Vorontsova, T. N., & Kuzmin, A. V. (1984). The distribution of new conodont species of the genus Polygnathus in the Famennian deposits of Central Kazakhstan. *Izv. Akad. Nauk SSSR, Ser. Geol, 10*, 58–64.

Walliser, O. H. (1984). Geologic processes and global events. *Terra Cognita, 4*, 17–20.

Webb, G. E. (2002). Latest Devonian and Early Carboniferous reefs: depressed reef building after the middle Paleozoic collapse. In: W., Kiessling, E., Flügel, J., Golonka. (Eds.). *Phanerozoic reef patterns. SEPM. Special Publications* 72, pp. 239–269.

Weddige, K. (1984). Zur Stratigraphie und Paläogeographie des Devons und Karbons von NE-Iran. *Senckenbergiana lethaea, 65,* 179–223.

Wendt, J., Kaufmann, B., Belka, Z., Farsan, N., & Karimi Bavandpur, A. (2002). Devonian/Lower Carboniferous stratigraphy, facies patterns and palaeogeography of Iran. Part I. Southeastern Iran. *Acta Geologica Polonica, 52*, 129–168.

Wendt, J., Kaufmann, B., Belka, Z., Farsan, N., & Karimi Bavandpur, A. (2005). Devonian/Lower Carboniferous stratigraphy, facies patterns and palaeogeography of Iran. Part II. Northern and Central Iran. *Acta Geologica Polonica, 55*, 31–97.

Yazdi, M. (1999). Late Devonian-Carboniferous conodonts from Eastern Iran. *RivistaItaliana di Paleontologiae Stratigrafa, 105*, 167–200.

Ziegler, W. (1962). Die Conodonten aus den Geröllen des Zechsteinkonglomerates von Rossenray (südwestlisch Rheinberg/Niederrhein). *Fortschritte in der Geologie von Rheinland und Westfalen, 6*, 391–406 pre-print 1960.

Ziegler, W. (1969). Eine neue Conodontenfauna aus dem höchsten Oberdevon. *Fortschritte Geologie von Rheinland und Westfalen, 17*, 179–191.

Ziegler, W., & Sandberg, C.A. (1984). Palmatolepis-based revision of upper part of standard Late Devonian conodont zonation, 179–194. In: D. L., Clarck (Ed.). Conodont biofacies and provincialism. *Geological Society of America Special Paper*, 196.

Ziegler, W., & Sandberg, C. A. (1990). The Late Devonian standard conodont zonation. *Courier Forschungsinstitut Senckenberg, 121*, 1–115.

Ziegler, W., & Sandberg, C. A. (1996). Reflexions on the Frasnian and Famennian stage boundary decisions as a guide to future deliberations. *Newsletters on Stratigraphy, 33*, 157–180.

Ziegler, W., & Sandberg, C. A. (2000). Utility of palmatolepids and icriodontids in recognizing Upper Devonian series, stages and possible substage boundaries. *Courier Forschungsinstitut Senckenberg, 225*, 335–437.

Ziegler, W., Sandberg, C. A., & Austin, R. L. (1974). Revision of Bispathodus group (Conodonta) in the Upper Devonian and Lower Carboniferous. *Geologica et Paleontologica, 8*, 97–112.